C.P. No. 264
(17,496)
A.R.C. Technical Report

C.P. No. 264
(17,496)
A.R.C. Technical Report

MINISTRY OF SUPPLY

AERONAUTICAL RESEARCH COUNCIL

CURRENT PAPERS

Boundary Layer Measurements on 10° and 20° Cones at M = 2.45 and Zero Heat Transfer

By

F. V. Davies and J. R. Cooke

LONDON: HER MAJESTY'S STATIONERY OFFICE

1956

PRICE 8s. 6d. NET

U.D.C. No. 532.526.2/4 : 533.691.18.011.5

Technical Note No. Aero 2314

November, 1954

ROYAL AIRCRAFT ESTABLISHMENT

Boundary layer measurements on 10° and 20° cones at M = 2.45 and zero heat transfer

by

F. V. Davies

and

J. R. 'ooke

SUMMARY

This note describes the measurement of boundary layers on two cones of total angles 10° and 20° in a supersonic airstream of M = 2.45 and under zero heat transfer conditions.

Transition from laminar to turbulent flow occurred between four and six inches from the tip of the 10° cone at a Reynolds number between 10^6 and 1.4×10^6; the layer on the 20° cone was laminar over its entire length of six inches, i.e. up to a Reynolds number of 1.4×10^6.

Most of the laminar boundary layer measurements were made on the 20° cone and results agree reasonably well with the flat plate solution of Monaghan[9] transformed by the theoretical cone-flat plate relations of Hantzsche and Wendt[4], and Mangler[5].

All the data for the turbulent boundary layer were obtained from measurements made on the 10° cone and comparison with flat plate data[2] indicates that the cone-flat plate relation is within 6 per cent of an empirical relation analogous to the $\sqrt{3}$ laminar boundary layer factor.

LIST OF CONTENTS

LIST OF APPENDICES

LIST OF ILLUSTRATIONS

LIST OF ILLUSTRATIONS (Contd)

1 Introduction

The investigation of the boundary layer characteristics of a body of revolution symmetrically placed in a uniform supersonic airstream can be regarded as a natural extension of work of a similar nature on flat plates[2,3]. A test programme was therefore set out to measure the boundary layer on cones and to correlate the results with those obtained for a flat plate. This note is concerned with a series of tests made with zero heat transfer conditions at the cone surface.

A single sided wooden nozzle designed for a nominal free stream Mach number of 2.48 was used for all tests, the cone being mounted axially on the centre line of the 5 inch square working section. Two cones were constructed for the tests, a hollow perspex cone of 10° total angle and a hollow copper cone of 20° total angle. The perspex cone was designed specifically for zero heat transfer tests. It was intended that the copper cone should be a development model for subsequent heat transfer cones, but it was considered that in addition useful comparisons could be made between results obtained from the two cones under zero heat transfer conditions. In practice however this comparison was restricted as the boundary layer over the entire surface of the 20° cone was laminar ($Re_x = 1.44 \times 10^6$), whereas transition occurred at about 4 inches from the tip of the 10° cone ($Re_x = 0.96 \times 10^6$). The investigation of the turbulent boundary layer was therefore entirely confined to the 10° cone, the bulk of the laminar boundary layer investigation being made on the 20° cone.

Temperature recovery factors were obtained from measurements on the 10° cone only and because of the small tip angle the thermocouple measurements were confined to the rear of the cone surface over which the boundary layer was turbulent.

2 Experimental apparatus

The tests described in this note were made using the same wind tunnel facilities as used in previous flat plate tests[1,2,3]. Modifications were made to the working section to take a cone mounting (fig.1) but no alterations to the instrumentation were necessary.

2.1 Cones and supports

The 10° perspex cone shown in figs. 2, 3 and 4 is 12 inches long and has an included angle of 10°. The body is moulded from 0.25 inch perspex sheet to form a hollow cone. The tip is stainless steel (tip radius 0.005 inch) to avoid erosion and extends for 2.5 inches of the cone length. There are six static pressure points (0.015 inch diameter) and the same number of copper constantan thermocouples made from 0.008 inch diameter wire, the positions being given in fig.2. Because of the small total angle of the cone it was not possible to locate the thermocouples closer to the tip than 5 inches. The thermocouple junctions were cemented into the holes with durofix and carefully positioned so as to be flush with the surface without being covered with cement.

The 20° copper cone (figs. 5, 6 and 7) is 6 inches long, the base diameter (due to blockage considerations) being the same as the 10° cone. It was made in the form of a conical shell 0.050 inch thick, the tip (radius 0.005 inch) being detachable. Static pressure points are positioned spirally around the cone at 90° intervals and in half inch steps (fig.5). They are formed from stainless steel hypodermic tubing "Easiflowed" into the shell.

Each cone has its own support and sting which are of similar pattern. The support is a machined forging of wedge section which spans the tunnel and is held in steel blocks in the side walls. The trailing edge is detachable and is in the form of a hollow wedge through which pressure tubes and thermocouples are led via the support blocks to the outside of the tunnel.

The cones are aligned in pitch by means of pitch alignment bars which are rigidly attached to the ends of the support. The cone is positioned visually with the aid of sighting wires and then locked into position with lock nuts. No provision is made for adjustment in yaw.

2.2 The tunnel working section

The working section (fig.1) is a single sided wooden nozzle with a window fitted into each side wall and is of similar construction and form to those used for the flat plate[1,2,3]. Holes for the pitot holder are spaced at intervals along the centre line of the profile wall. The original nozzle was constructed with these holes offset $\frac{3}{8}$ inch from the centre line to reduce interference from the pitot support tube when traversing the centre line. The interference was found to be negligible and because of the inconvenience of using cranked tubes a new nozzle was made with holes on the centre line. Pitot holders were drilled so that the movement of the pitot is normal to the surface of the cone.

2.3 Tunnel calibration

The nozzle (an adaptation of a Kochel nozzle) was designed to give a nominal free stream Mach number of 2.48. Static pressure measurements on the flat wall of the nozzle indicated an average free stream Mach number in this region of 2.45 with a variation of ± 0.5 per cent. Flow conditions in the vicinity of the cone were obtained from measurements of total pressure and temperature just upstream of the nozzle and from static pressures on the cone surface. The Mach number distributions along the top generators of the cones are shown in fig.10 indicating a variation of ± 1 per cent and good agreement with the theoretical values.

3 Potential flow over cones

The potential flow over a cone in a supersonic stream is non-uniform and thus for integration of certain boundary layer functions normal to the surface it is important to define 'free stream' conditions immediately outside the layer.

Taylor and Macoll have demonstrated theoretically that the potential flow field around a cone in a supersonic flow is one in which the parameters pressure, density and velocity are all constant over conical surfaces lying between the cone surface and the attached Mach cone and having vertices coincident with that of the cone. M.I.T. have produced numerical solutions[6] and from these Mach number distributions are plotted in figs. 9 and 10.

The potential flow distribution shown in fig.9 for a 10° cone shows that within 3 boundary layer thicknesses of the outer edge of the layer there is a variation of 0.15 per cent in the Mach number distribution (the presence of the boundary layer itself will alter the overall level of the Mach number by about 2 per cent). This velocity gradient is so small as to have little or no effect on the definition of the edge of the boundary layer and there is no practical difficulty in selecting free stream boundary conditions. (It is difficult to compare the experimental variation with the theoretical one but pitot traverses indicate that measured changes in Mach number are no larger than the corresponding theoretical values.)

The theoretical values of the Mach number M_1 just outside the boundary layer are shown in fig.10 and overestimate the measured values by between 1 and 2 per cent. The former are uncorrected for the presence of the boundary layer and for the purposes of calculation the following values of M_1 are used

$$10^\circ \text{ cone}, \qquad M_1 = 2.35$$

$$20^\circ \text{ cone}, \qquad M_1 = 2.23 .$$

4 The boundary layer: general definitions and measurements

4.1 Boundary layer definitions

The characteristics of the boundary layer are described below:

Displacement thickness
$$\delta^* = \int_0^\delta \left(1 - \frac{\rho u}{\rho_1 u_1}\right) dy \qquad (1)$$

Momentum thickness
$$\theta = \int_0^\delta \frac{\rho u}{\rho_1 u_1}\left(1 - \frac{u}{u_1}\right) dy \qquad (2)$$

Shape parameter
$$H = \frac{\delta^*}{\theta} \qquad (3)$$

where ρ is the density in the boundary layer

u is the velocity in the boundary layer parallel to the surface

y is the ordinate measured perpendicular to the surface (in this case the cone surface)

δ is the boundary layer thickness

and subscript 1 refers to free stream conditions.

The values of δ^* and θ are calculated from experimental readings in a manner similar to that described in ref.2.

For zero pressure gradient along the cone surface the local skin friction coefficient is given by

$$c_f = \frac{\tau_w}{\frac{1}{2}\rho_1 u_1^2} = 2\frac{d\theta}{dx} + \frac{2\theta}{x} . \qquad (4)$$

(The corresponding flat plate equation is $c_f = 2\frac{d\theta}{dx}$)

where x is the distance measured along a cone generator from the tip

$\tau = \mu \frac{du}{dy}$ (μ is the viscosity)

subscript w refers to conditions at $y = 0$.

By integrating equation (4) along the cone surface from the tip to position 'x' the total skin friction coefficient is given by

$$C_F = \frac{F}{\frac{1}{2}\rho_1 u_1^2 S} = \frac{4\theta}{x} . \qquad (5)$$

(The corresponding flat plate equation is $C_F = \frac{2\theta}{x}$)

where F is the overall viscous force experienced by a section of the cone

S is the corresponding wetted area.

4.2 Boundary layer measurements

Boundary layer characteristics on cones were obtained from measurements of total pressure in the boundary layer, static pressures at the cone surface and from surface temperature measurements with thermocouples fitted flush with the surface of the cone. Pitot pressures were measured through the layer with small bore steel or quartz tubes.

Transition from laminar to turbulent flow was detected by measuring pitot pressures along a cone generator. This was carried out by means of a 'creeper' tube which enables a continuous traverse to be made parallel to the surface. The boundaries between laminar and transition regions, transition and turbulent regions are characterised by marked changes in total pressure (see fig.15).

4.21 Effects of pitot size on the measurement of the boundary layer

The effects of pitot size were confined almost entirely to the laminar boundary layer. With boundary layer thicknesses of the order of 0.030 inch (at transition on the 10° cone and at the rear of the 20° cone) the relative inaccuracies in measurement were also found to be of greater significance for the laminar boundary layer than for the turbulent layer.

The size effects are described in detail in ref.7 and it was found that apparent distortions in the boundary layer arising from measurements with pitot tubes could be related to the parameters $\left(\frac{d}{\delta}\right)$ and $\left(\frac{ud}{\nu}\right)$ (where δ is the boundary layer thickness and $\left(\frac{ud}{\nu}\right)$ is a Reynolds number based on local conditions within the boundary layer and the tube diameter d). It was found[7] that to avoid appreciable errors in the calculation of δ^* and θ from experimental data, observation of the rough criterion $\left(\frac{d}{\delta}\right) < 0.2$ was sufficient; the parameter $\left(\frac{ud}{\nu}\right)$ was less important in this respect. However, boundary layer measurements described in this note and the size effects of ref.7 were carried out to a large extent in parallel and it was not possible therefore to fully utilize the findings of ref.7 in the planning of this test series. It is useful however to compare present results on a $\frac{d}{\delta}$ basis and the experimental data have been divided into two parts, the first obtained from pitot traverses falling into the category $\frac{d}{\delta} > 0.3$, the second obtained from pitot traverses falling into the category $\frac{d}{\delta} < 0.3$. (The limit has been arbitrarily raised for the present test series because of the relatively small proportion of pitot traverses which come into the category $\frac{d}{\delta} < 0.2$.)

Points plotted on graphs taken from data conforming to $\left(\frac{d}{\delta}\right) < 0.3$ are termed 'limit points' and show less scatter than those in the former group.

This is not an entirely satisfactory way of dealing with these size effects but in future it is intended where possible to select pitots so that the $\frac{d}{\delta}$ value is approximately the same for all traverses.

5 The laminar boundary layer

It has been shown theoretically by Hantzsche and Wendt[4], and Mangler[5] that a simple relation exists between the laminar boundary layer solution on a cone and the corresponding solution on a flat plate (see para. 5.3). Experimental results obtained on the 10° and 20° cones are therefore compared directly with

(a) an approximate flat plate solution[9] by Monaghan,

(b) flat plate results obtained from tests[2,3] in the same tunnel.

5.1 Experimental results

Measured velocity profiles over the forward portion of the cone are shown in fig.11. The profiles for the 10° cone were obtained from pitot traverses having considerably larger $\frac{d}{\delta}$ ratios than those for the 20° cone and are not so consistent.

Creeper traverses show transition to commence at $x = 4$ inches ($Re_x = 0.96 \times 10^6$) on the 10° cone (fig.15) and not at all on the 20° cone. This is not inconsistent with the trends shown by the velocity profiles.

Figs. 12 and 13 show the variation of displacement and momentum thicknesses for 10° and 20° cones. The experimental points can be represented by the following equations:

10° cone

$$\delta^* = 3.18 \, (Re_x)^{-\frac{1}{2}} \, x \qquad (6)$$

$$\theta = 0.49 \, (Re_x)^{-\frac{1}{2}} \, x \qquad (7)$$

20° cone

$$\delta^* = 2.30 \, (Re_x)^{-\frac{1}{2}} \, x \qquad (8)$$

$$\theta = 0.42 \, (Re_x)^{-\frac{1}{2}} \, x \, . \qquad (9)$$

5.2 Comparison between the cone experimental results and a laminar boundary layer approximate solution[9]

Theoretical equations corresponding to equations (6), (7), (8) and (9) are for

10° cone ($M_1 = 2.35$)

$$\delta^* = 2.445 \, (Re_x)^{-\frac{1}{2}} \, x \qquad (10)$$

$$\theta = 0.371 \, (Re_x)^{-\frac{1}{2}} \, x \qquad (11)$$

20° cone ($M_1 = 2.23$)

$$\delta^x = 2.30\ (Re_x)^{-\frac{1}{2}}\ x \qquad (12)$$

$$\theta = 0.371\ (Re_x)^{-\frac{1}{2}}\ x\ . \qquad (13)$$

These are obtained from Monaghan's flat plate laminar boundary layer approximate solution[9] transformed by theoretical flat plate-cone boundary layer relations (para. 5.3 and Appendix I). Direct comparison is made between the theoretical curves and experimental points in figs. 12 and 13. In Table I below, however, results are corrected to a Mach number of 2.35 (see Appendix V).

Table I

A comparison between the experimental and theoretical laminar boundary layer functions for supersonic flow over 10° and 20° cones

Boundary Layer Function	Comparison between Experimental Data and a Laminar Boundary Layer Approximate Solution[9]			
	Theoretical	Experimental		
		10° cone	20° cone	20° 'Limit Points'
$\delta^x\ Re_x^{\frac{1}{2}}\ x^{-1}$	2.445	3.18	2.54	2.21
$\theta\ Re_x^{\frac{1}{2}}\ x^{-1}$	0.371	0.49	0.42	0.39
H	6.61	6.5	6.06	5.65

Experimental data have been corrected where necessary to conditions corresponding to $M_1 = 2.35$. The test Mach numbers immediately outside the boundary layer are $M_1 = 2.35$ for the 10° cone and $M_1 = 2.23$ for the 20° cone.

These comparisons show that agreement between the results from the 20° cone and the approximate solution are reasonably good. The 10° cone results show a boundary layer growth much in excess of that predicted by theory. Greater reliance can be placed on the results from the 20° cone because of the superior tip joint and because the effects of pitot size on the measurements are much less marked. The d/δ ratios were much smaller for traverses on the 20° cone than those for the 10° cone and this is reflected in reduced scatter and greater accuracy in the 20° cone results.

5.3 Comparisons between measured cones and flat plate boundary layers

Before comparing the experimental results of the cones and flat plate[2] it is convenient to state the theoretical relations derived by Hantsche and Wendt[4], and Mangler[5]. The boundary layer equations, for a flat plate and a body of revolution in a uniform supersonic flow are shown to be simply related by a function of the co-ordinates of the body of revolution. For a cone the function is independent of cone angle and becomes the simple factor shown in the cone-flat plate relations given overleaf:

Displacement thickness

$$\frac{[\delta^{x}(Re_x)^{\frac{1}{2}} x^{-1}]_c}{[\delta^{x}(Re_x)^{\frac{1}{2}} x^{-1}]_p} = \frac{1}{\sqrt{3}} \qquad (14)$$

Momentum thickness

$$\frac{[\theta(Re_x)^{\frac{1}{2}} x^{-1}]_c}{[\theta(Re_x)^{\frac{1}{2}} x^{-1}]_p} = \frac{1}{\sqrt{3}} \qquad (15)$$

Local skin friction

$$\frac{[c_f(Re_x)^{\frac{1}{2}}]_c}{[c_f(Re_x)^{\frac{1}{2}}]_p} = \sqrt{3} \qquad (16)$$

Overall skin friction

$$\frac{[C_F(Re_x)^{\frac{1}{2}}]_c}{[C_F(Re_x)^{\frac{1}{2}}]_p} = \frac{2}{3}\sqrt{3} \qquad (17)$$

where subscripts c and p refer to cone and flat plate respectively.

Corresponding relations derived from test results of the 10° and 20° cones and the flat plate show considerable divergence from the theoretical relations and no real conclusions can be drawn. This lack of agreement and consistency should be considered with the following facts in mind. Tests on the flat plate and 10° cone were carried out with the emphasis on the measurement of the turbulent boundary layer, measurement of the laminar boundary layer being of a more incidental nature. Only in tests on the 20° cone was special attention paid to flow conditions in the tip region and to the effects of pitot size on boundary layer measurements.

5.4 The shape parameter H

Experimental values of $H = \frac{\delta^{x}}{\theta}$ are shown in fig.14. Data for the laminar boundary show a large amount of scatter and are in general overestimated by theory. The values of H (for the laminar layer) for the 10° cone tend to increase with x, but those for the 20° cone do not vary appreciably with x.

5.5 Skin friction

The overall skin friction coefficient C_F is plotted against Reynolds number in fig.18, and except for a few 'limit points' experimental data are underestimated by the theoretical curve.

5.6 Some conclusions regarding the laminar boundary layer results

Conclusions regarding the laminar boundary layer results may be summarised as follows. Theoretical results obtained from the approximate

solution[9] of Monaghan and the $\sqrt{3}$ theoretical cone-flat plate transformation factors are reasonably supported by experimental results from the 20° cone.

Experimental results from the 10° cone and the flat plate tests are less satisfactory because of the incidental nature of the laminar boundary layer investigation in these two cases. Cone-flat plate relations obtained from comparisons based entirely on experimental results from 10° and 20° cone and flat plate tests are therefore not reliable and do not support the theoretical $\sqrt{3}$ factors.

It is clear from the previous paragraphs that the accurate measurement of the laminar boundary layer of the order of thickness described in this note requires considerable care and attention to detail. Particular attention must be paid to the smoothness of the forebody, the profile of the tip or leading edge and flow conditions at the model entry. Scatter of the measured results may be reduced by greater control of pitot size - pitots should conform as closely as possible to the limits proposed in ref.7.

6 Transition from a laminar to a turbulent boundary layer

The position of the transition was determined by means of a creeper traverse along the surface of the cones. For zero heat transfer conditions the boundary layer on the 20° cone was laminar over the entire surface. Transition occurred under these conditions on the 10° cone and a surface pitot pressure plot is shown in fig.15.

This indicates that the layer is laminar from the tip to $x = 4"$, that transition extends over the range $(4" < x < 5.7")$ the layer thereafter being turbulent. The transition region corresponds to a Reynolds number range based on x of $(0.96 \times 10^6 < Re_x < 1.37 \times 10^6)$. This is supported by the plots of displacement and momentum thickness (figs. 12 and 13) and shapes of the velocity profiles in the transition region. The velocity profiles show clearly that for $x = 6.0"$ (fig.11a) the departure from the laminar profile is very marked; similarly at $x = 5.5"$ (fig.16) the departure from the turbulent profile is large.

7 Turbulent boundary layer

The measured turbulent boundary layer on the 10° cone (the boundary layer on the 20° cone is entirely laminar for zero heat transfer conditions) is interpreted on

(a) a power law velocity profile basis (para. 7.1), leading to

(b) a log law velocity profile basis (para. 7.2).

Cone-flat plate turbulent boundary relations are obtained from experimental data from 10° cone and flat plate tests. These are compared with results from two semi theoretical analyses by Young[12] and Van Driest[13].

7.1 Velocity profile analysis (Power Law velocity profiles)

Some typical velocity profiles are shown in fig.16 and are compared with 1/6th, 1/7th and 1/8th profiles of the type

$$\frac{u}{u_1} = \left(\frac{y}{\delta}\right)^{\frac{1}{n}}$$

$$= \left(\frac{y}{\delta^x}\right)^{\frac{1}{n}} \left(\frac{\delta^x}{\delta}\right)^{\frac{1}{n}} \quad * \qquad (18)$$

where n can be 6, 7, 8 etc.

The measured profiles are not perfectly represented by a power law profile, but the 1/7th power law is probably the best and analysis of the data on the basis of this profile is considered justifiable.

7.11 Displacement and momentum thicknesses

The experimental velocity profiles being represented by the 1/7th power law, we shall assume that the displacement and momentum thicknesses are given as in incompressible flow by

$$\delta^x = A\,(Re_X)^{-1/5}\,X \qquad (19)$$

$$\theta = B\,(Re_X)^{-1/5}\,X \qquad (20)$$

where $X = x - C$, C being the distance between the origin of the laminar boundary layer and the effective start of the turbulent layer.

Equations (19) and (20) may be rearranged to be linear in X (or x)

$$\delta^{x\,5/4}\left(\frac{u_1}{\nu_1}\right)^{\frac{1}{4}} = A^{5/4}\,X \qquad (21)$$

$$\theta^{5/4}\left(\frac{u_1}{\nu_1}\right)^{\frac{1}{4}} = B^{5/4}\,X \qquad (22)$$

where ν is the kinematic viscosity $\left(\frac{\mu}{\rho}\right)$ and subscript 1 refers to conditions at the edge of the boundary layer.

Experimental results are first plotted in this form (fig.17). Linear laws for each set of experimental points are obtained by the method of Least Squares and values for A, B and C obtained. In fact four constants A, B, C and C' are obtained, two for each equation. Evaluation of these constants gives

---

* δ^x, θ and δ are related by the integrals

$$\delta^x = \int_0^\delta \left(1 - \frac{\rho u}{\rho_1 u_1}\right) dy \qquad \theta = \int_0^\delta \frac{\rho u}{\rho_1 u_1}\left(1 - \frac{u}{u_1}\right) dy \qquad \text{(para.4).}$$

These integrals are determined in ref.10 in terms of δ with the free stream Mach number and index n as parameters.

For zero heat transfer, $M_1 = 2.35$ and $n = 7$

$$\delta = 3.72\,\delta^x \quad \text{and} \quad \delta = 13.9\,\theta.$$

$$\delta^{x} = 0.0566\left(\frac{u_1 X_\delta}{\nu_1}\right)^{-1/5} X_\delta \qquad (23)$$

$$\theta = 0.0165\left(\frac{u_1 X_\theta}{\nu_1}\right)^{-1/5} X_\theta \qquad (24)$$

where $X_\delta = x - 1.72$

$X_\theta = x - 2.77$.

The effective start of the turbulent boundary layer is usually taken to be the position at which the momentum thickness is zero. This is given by equation (24) and occurs when $X_\theta = 0$ or $x = 2.77$.

7.12 Boundary layer thickness

The relations between the boundary layer thickness δ, the displacement thickness δ^{x} and the momentum thickness θ are given in para. 7.1. Using equations (23) and (24) two expressions for δ can be obtained

$$\delta = 0.211\left(\frac{u_1 X_\delta}{\nu_1}\right)^{-1/5} X_\delta \qquad (25)$$

$$\delta = 0.229\left(\frac{u_1 X_\theta}{\nu_1}\right)^{-1/5} X_\theta \qquad (26)$$

the former being derived from the equation for displacement thickness and the second from the equation for momentum thickness.

Taking an arithmetic mean of the constants for these equations and assuming x large so that $X_\theta \approx X_\delta \approx x$, then

$$\delta_c = 0.22\left(\frac{u_1 x}{\nu_1}\right)^{-1/5} x \qquad (27)$$

where subscript c refers to cone in compressible flow.

The comparable equation for incompressible flow over a flat plate is

$$\delta_{p_i} = 0.37\left(\frac{u_1 x}{\nu_1}\right)^{-1/5} x \qquad (28)$$

where subscript p_i refers to flat plate in incompressible flow.

Evidence from ref.2 indicates that the boundary layer thickness for a flat plate at $M = 2.45$ is also given by equation (28), i.e.

$$\delta_{p_c} = 0.37\left(\frac{u_1 x}{\nu_1}\right)^{-1/5} x \,. \qquad (29)$$

Comparison between equations (27) and (29) relates the cone and flat plate boundary layers in compressible flow, i.e.

$$\frac{\delta_c}{\delta_p} = \frac{1}{1.68} . \qquad (30)$$

This is within 3 per cent of the theoretical laminar relation

$$\frac{\delta_c}{\delta_p} = \frac{1}{\sqrt{3}} .$$

Provided the $\sqrt{3}$ laminar factor is accepted as applicable to the turbulent boundary layer (this is discussed in detail in para. 7.2), then support is given to the conclusion reached in ref.2 that there is little variation in the boundary layer thickness in changing from incompressible flow to a Mach number of 2.5.

7.13 Skin friction

The mean skin friction is given by

$$C_F = \frac{F}{\frac{1}{2}\rho_1 u_1^2 S} = \frac{4\theta}{x} . \qquad (31)$$

The experimental data is represented by the mean curve (equation (24))

$$C_F = 0.066 \left(\frac{u_1 x}{\nu_1}\right)^{-1/5} \left(\frac{x_\theta}{x}\right)^{4/5} . \qquad (32)$$

This is shown in fig.18 together with the asymptote

$$C_F = 0.066 \left(\frac{u_1 x}{\nu_1}\right)^{-1/5} . \qquad (33)$$

7.2 Log law profile analysis

The general log law profile

$$\frac{u}{u_\tau} = A + B \log_{10} y_\tau \qquad (34)$$

where $u_\tau = \sqrt{\frac{\tau_o}{\rho}}$ and $y_\tau = \frac{u_\tau y}{\nu}$, τ_o being the local skin friction, is used as a basis on which to interpret results (fig.19). Experimental points were plotted using density and viscosity evaluated at free stream conditions. The local skin friction is given by

$$\tau_o = \rho_1 u_1^2 \left\{\frac{d\theta}{dx} + \frac{\theta}{x}\right\}$$

the terms inside the bracket being obtained from the mean curve in fig.13. Three profiles (at $x = 7.6$ ins, 9.0 ins and 10.1 ins) are given in fig.19. The profiles at $x = 7.6$ ins and 9.0 ins are consistent. Agreement with the profile at $x = 10.1$ ins is not as good but all three profiles may be reasonably represented by the mean curve

$$\frac{u}{u_{\tau_w}} = 4.93 + 5.56 \log_{10} y_{\tau_w} \qquad (35)$$

where $u_{\tau_w} = \sqrt{\frac{\tau_o}{\rho_w}}$ and $y_{\tau_w} = \frac{u_{\tau_w} y}{\nu_w}$

the subscript w referring to conditions at the surface.

For comparison the representative curves of ref.2 and ref.3 are also shown in fig.19

$$\frac{u}{u_{\tau_w}} = 5.5 + 5.75 \log_{10} y_{\tau_w} \quad \text{(ref.2)} \qquad (36)$$

(the profile deduced from incompressible pipe flow) and

$$\frac{u}{u_{\tau_w}} = 5.45 + 5.40 \log_{10} y_{\tau_w} \qquad (37)$$

(the profile obtained experimentally from flat plate results at zero heat transfer in ref.3).

Present results show better agreement with the profile of ref.3 (equation (37)).

7.21 The shape parameter H

A relation between the compressible and incompressible flow leading from the assumption of the log law profile is

$$\frac{H}{H_i} = \frac{T_w}{T_1} + 0.2 M_1^2 \quad \text{(ref.2)} \qquad (38)$$

$$= 1 + 0.379 M_1^2 \quad \text{(for zero heat transfer conditions)}$$

$$= 3.09 \quad \text{for} \quad M_1 = 2.35.$$

A more recent equation[3] is

$$\frac{H}{H_i} = \frac{T_w}{T_1} + \sigma^{\frac{1}{3}} \frac{(\gamma - 1)}{2} M_1^2 \qquad (39)$$

$$= 1 + 0.36 M_1^2$$

$$= 2.99 \quad \text{for} \quad M_1 = 2.35.$$

Taking a value of $H_i = 9/7$, values for H are

$H = 3.97$ from equation (38)

$H = 3.84$ from equation (39).

These are shown in fig.14.

The power law value of $H = 3.43$ is derived from the definition

$$H = \frac{\delta^*}{\theta}$$

and the equations (23) and (24). This is in fact the asymptote to which the experimental values of H tend as x tends to infinity. It might be inferred therefore that equations (38) and (39) overestimate H, but the length of run of the turbulent boundary layer is insufficient to make this a firm conclusion.

7.3 Relating the turbulent boundary layers on a cone and a flat plate

Because of the present incomplete state of the turbulent boundary layer theory no rigorous mathematical relations can be derived between the turbulent boundary layers on cones and flat plates.

Two semi-theoretical analyses have been made by Van Driest[13] and Young[12]. These are discussed in Appendices II and III, where Van Driest's analysis is extended to remove an apparent inconsistency in the order (mathematical) of his results. The formulae obtained by application of these analyses are given in sections 7.311 and 7.312. Section 7.313 considers the implications of using a "laminar type" relation.

Numerical values are given in Table II at the end of this section, where they are compared with the present test results. The comparison is discussed in sections 7.32 and 7.33.

7.31 Theoretical relations between cone and flat plate boundary layers

7.311 Comparison assuming similar log law profiles (extension of Van Driest's analysis[13])

The assumption is made that the log law profile

$$\frac{u}{u_{\tau_w}} = A + B \log_{10} y_{\tau_w} \qquad (40)$$

$$\left(\text{or} \quad \frac{u}{u_{\tau_w}} = D + \frac{1}{k} \log_e y_{\tau_w} \right)$$

will apply to the cone and flat plate boundary layers with the same values for the constants A and B. This is in fact borne out by experimental data (see section 7.2). Application of the momentum equation indicates that the cone and flat plate relations for skin friction are the same when the Reynolds numbers are related by

$$\frac{(Re_x)_c}{(Re_x)_p} = 2\left\{1 + \frac{3}{2}\frac{1}{ks}\right\} \qquad (41)$$

(omitting terms of $0\left(\frac{1}{s^2}\right)$ and less, see Appendix II)

where $s = \sqrt{\frac{2}{c_{f_w}}}$

and $c_{f_w} = \frac{\tau_o}{\frac{1}{2}\rho_w u_1^2}$.

The corresponding result of Van Driest[13] is that the relations for skin friction are similar when the Reynolds number on the cone is twice

that of the flat plate. The log law result contains an additional term $\frac{3}{ks}$ which makes an appreciable difference to the results for conditions considered in this note. Taking the modified Blasius formula for flat plate skin friction[14]

$$\frac{c_{f_w}}{2} = 0.0296 \left(Re_w \frac{T_1}{T_w} \right)^{-1/5} \tag{42}$$

and the incompressible value of $k = 0.4$ then at $M_1 = 2.35$, under zero heat transfer conditions and for $(Re_x)_p = 10^6$ $\frac{(Re_x)_c}{(Re_x)_p} = 2.39$. The variation of the Reynolds number relation (equation (41)) with $(Re_x)_p$ is shown in fig.20.

For the same Reynolds number, Mach number on cone and flat plate and for zero heat transfer conditions the results given below follow:

$$\frac{c_{f_c}}{c_{f_p}} = \left[2 \left\{ 1 + \frac{3}{2} \frac{1}{ks} \right\} \right]^{1/5} \tag{43}$$

$$\frac{\theta_c}{\theta_p} = \left[2 \left\{ 1 + \frac{3}{2} \frac{1}{ks} \right\} \right]^{-4/5} \tag{44}$$

$$\frac{C_{F_c}}{C_{F_p}} = 2 \left[2 \left\{ 1 + \frac{3}{2} \frac{1}{ks} \right\} \right]^{-4/5}. \tag{45}$$

Values of $\frac{c_{f_c}}{c_{f_p}}$, $\frac{\theta_c}{\theta_p}$ and $\frac{C_{F_c}}{C_{F_p}}$ are included in Table II for $(Re_x)_p = 10^6$.

7.312 Comparison using an extension of Young's analysis[12]

The analysis of Young assuming the power law

$$\frac{\tau_o}{\rho_1 u_1^2} = C \left(\frac{u_1 \theta}{\nu_1} \right)^{-\frac{1}{n-1}} \tag{46}$$

leads to the result that the relation between turbulent boundary layers on a flat plate and a cone is solely a function of the exponent n (Appendix III). The variation of n within normal limits (i.e. corresponding to velocity profile changes from $1/5$ to $1/9$) produces changes in the boundary layer relations of only ± 2 per cent. The relations corresponding to the $1/7$th power law velocity profile are given in Table II the variation of these factors with n being shown in Fig.21.

7.313 The empirical 'laminar' type relations

The assumptions in this case are that for similar Reynolds numbers the thicknesses of the turbulent boundary layers on a cone and a flat plate may be related by a constant, and that the momentum thickness is given by

$$\theta = \text{const } (Re_x)^{-\frac{1}{n}} x .$$

It follows that the mean skin friction relation is constant (cf. section 4.1) but the local skin friction relation is dependent upon the exponent n (Appendix II). The results shown in Table II are for a boundary layer thickness ratio of $1/\sqrt{3}$ (i.e. the same as for the laminar layer) and for a $1/7$th power law velocity profile (i.e. n = 5).

7.32 Comparison of cone flat plate experimental results

Experimental results obtained from the 10° cone (section 7.1) are compared in Table II with the flat plate results of ref.2 on a power law basis. Mach number corrections (Appendix V) similar to those made for flat plate laminar boundary layer results are made to the flat plate results as given in Table II.

7.33 Comparisons between the experimental cone-flat plate relations and those derived from theory

The theoretical and experimental relations discussed in the previous paragraphs are compared in Table II. There is no direct support for either the 'semi theoretical' analysis or the empirical relations. An overall conclusion is that comparing the turbulent boundary layer on a cone with that on a flat plate, the measured rate of growth and skin friction are larger than that predicted by theory. Although the empirical 'laminar' type relations most nearly approach the experimental values, the consistency of that of the measured log law profiles for the 10° cone and the flat plate suggest that the initial assumptions of the log law analysis have the strongest support from present experimental data.

The choice of a suitable function by which the turbulent boundary layers on flat plates and cones may be related is therefore in doubt until further experimental data are available. Meantime, although the log law analysis has a sounder physical basis the tentative adoption of the empirical 'laminar' relations is to be preferred.

/Table II

Table II

A comparison of experimental turbulent boundary layer functions for supersonic flow over a flat plate[2] and the 10° cone with some 'semi theoretical' functions

Boundary Layer Function	Flat Plate (Corrected to $M_1 = 2.35$)	10° cone	Cone/Flat Plate Experimental Relations	Cone/Flat Plate Relations Derived from a Log Law Analysis (Appendix II) (Values for $(Re_x)_p = 10^6$) Section 7.311	Cone/Flat Plate Relations Derived from Young's Analysis (Appendix III) Section 7.312	Cone/Flat Plate Empirical Relations (Appendix IV) Section 7.313
δ^*	0.102	0.0566	$\frac{1}{1.80}$	$\frac{1}{2.01}$	$\frac{1}{1.91}$	$\frac{1}{\sqrt{3}} = \frac{1}{1.73}$
θ	0.027	0.0165	$\frac{1}{1.64}$	$\frac{1}{2.01}$	$\frac{1}{1.91}$	$\frac{1}{\sqrt{3}} = \frac{1}{1.73}$
c_f	0.043	$0.033\{0.8 + \frac{x}{x}\}$ $\rightarrow 0.0594$ as $\frac{x}{x} \rightarrow 1$	1.38	1.19	1.176	$\frac{3}{4}\sqrt{3} = 1.30$
C_F	0.054	0.066	1.22	0.995	1.045	$\frac{2}{3}\sqrt{3} = 1.16$

The term cone/flat plate relations refers to $\frac{\delta^*_c}{\delta^*_p}$ etc. for corresponding values of x and Reynolds number. Subscripts c and p refer to cone and flat plate respectively.

8 Temperature recovery factors on the 10° cone

The recovery factor β is the ratio of the temperature rise in the boundary layer with zero heat transfer to the corresponding adiabatic rise, i.e.

$$\beta = \frac{T_{w_o} - T_1}{T_o - T_1} . \tag{47}$$

Recovery factors were obtained experimentally by measuring the stagnation temperature T_o upstream of the throat with both a mercury thermometer and a thermocouple, and under zero heat transfer conditions measuring the boundary temperature T_{w_o} at the surface by means of six copper constantan thermocouples installed as shown in fig.2. The static temperature T_1 was evaluated from the energy relation

$$\frac{T_o}{T_1} = \left\{ 1 + \frac{\gamma-1}{2} M_1^2 \right\} . \tag{48}$$

The experimental data together with the positions of the thermocouples are given in fig.22. The two sets of points in the turbulent region (thermocouples 5 and 6) give an average recovery factor $\beta = 0.888$ which is a little below the formula given by Squire[11] for the recovery factor of a turbulent boundary layer

$$\beta = (\sigma)^{\frac{1}{3}} = \left(\frac{\mu C_p}{k} \right)^{\frac{1}{3}} \tag{49}$$

where σ is the Prandtl number (taken as 0.72 for air)

C_p the specific heat at constant pressure

k the thermal conductivity

i.e. $\beta = 0.72^{\frac{1}{3}} = 0.896$.

Thermocouples 1, 2, 3 and 4 are in the transition region and measurements show considerable scatter; this may be due to asymmetry in the transition position around the cone. It was not possible to install thermocouples nearer to the cone tip than 4.9 inches because of the small vertex angle of the cone and no direct comparison with the theoretical laminar recovery factor

$$\beta = (\sigma)^{\frac{1}{2}} \tag{50}$$

$$= 0.72^{\frac{1}{2}} = 0.849$$

is possible. There is, however, some indication from the transition values that the recovery factor approaches the theoretical value in the laminar region.

9 Conclusions

Consideration of data from tests on the 10° and 20° cones at $M_\infty = 2.45$ and under zero heat transfer conditions allows the following conclusions to be drawn:

(1) The boundary layer on the 10° cone is turbulent for $Re_x > 1.4 \times 10^6$ but at this Reynolds number on the 20° cone laminar flow is still maintained. This is thought to be due to differences in surface finish (particularly at the tip joints) between the two cones.

(2) The measured laminar boundary layer on the 20° cone agrees fairly well with Monaghan's approximate flat plate theory[9] transformed by the theoretical cone-flat plate factors derived by Hantzsche and Wendt[4], and Mangler[5].

(3) The measured turbulent boundary layer on the 10° cone has been analysed on a power law basis and a log law basis. In the former case the velocity profiles are in closest agreement with the 1/7th power law profile. In the latter case the skin friction velocity profiles are consistently represented by the log law

$$\frac{u}{u_{\tau_w}} = A + B \log_{10} y_{\tau_w}$$

the constants being $A = 4.93$ and $B = 5.56$. This is in reasonable agreement with the log law representation of the flat plate profiles of ref.3 in which $A = 5.45$ and $B = 5.40$.

The correspondence between the turbulent boundary layer on a cone and that on a flat plate is examined on the following bases:

(i) a comparison of measured boundary layers on a cone (this note) and a flat plate (ref.2), the data being reduced on a power law basis;

(ii) a log law analysis similar to that of Van Driest[13];

(iii) a power law analysis by Young[12];

(iv) empirical relations analogous to the $\sqrt{3}$ laminar boundary layer factors.

Agreement between the measured skin friction profiles for the 10° cone and the flat plate supports the basic assumption of the log law analysis. However, factors derived from the experimental data do not completely support any one of the theories (Table II) but until further experimental data are available it is suggested that the empirical 'laminar' factors set out below are sufficiently accurate (within 6 per cent of the measured factors) to be used for engineering purposes. The factors are:

$$\frac{\left[\delta^* (Re_x)^{1/5_x-1}\right]_c}{\left[\delta^* (Re_x)^{1/5_x-1}\right]_p} = \frac{1}{\sqrt{3}}$$

$$\frac{\left[\theta (Re_x)^{1/5_x-1}\right]_c}{\left[\theta (Re_x)^{1/5_x-1}\right]_p} = \frac{1}{\sqrt{3}}$$

$$\frac{\left[c_f (Re_x)^{1/5}\right]_c}{\left[c_f (Re_x)^{1/5}\right]_p} = \frac{3}{4}\sqrt{3}$$

$$\frac{[C_F (Re_x)^{1/5}]_c}{[C_F (Re_x)^{1/5}]_p} = \frac{2}{3}\sqrt{3} .$$

(4) Recovery factors for the turbulent boundary layer measured by surface thermocouples on the 10° cone are in reasonable agreement (average experimental value $\beta = 0.888$) with the accepted value $\beta = (\sigma^{\frac{1}{3}}) = 0.896$ for $\sigma = 0.72$. No measurements were possible in the laminar region because of thermocouple installation difficulties near the tip of the cone.

List of Symbols

x distance along cone generator from tip

y distance normal to cone surface

r_o radius of axi-symmetric body

u velocity at a point in the boundary layer parallel to the surface

u_1 velocity immediately outside the boundary layer

v velocity at a point in the boundary layer normal to the surface

T_o stagnation temperature of the flow

T_1 static temperature of the stream immediately outside the boundary layer

T_{w_o} temperature of the boundary layer at the surface

T_w the temperature of the wall

ρ density (subscripts as for temperature)

μ dynamic viscosity

ν kinematic viscosity (subscripts as for temperature)

Re_x Reynolds No. based on length x, with free stream viscosity and velocity

δ thickness of boundary layer

δ^* displacement thickness of the boundary layer $= \int_o^\delta \left(1 - \frac{\rho u}{\rho_1 u_1}\right) dy$

θ momentum thickness of the boundary layer $= \int_o^\delta \frac{\rho u}{\rho_1 u_1}\left(1 - \frac{u}{u_1}\right) dy$

τ local skin friction

F total skin friction on length x, $= \int_o^x \tau_o \, dx$

List of Symbols (Contd)

c_f local skin friction coefficient

$$= \frac{\tau_o}{\frac{1}{2}\rho_1 u_1^2} = \frac{\left(2\frac{d\theta}{dx} + 2\frac{\theta}{x}\right)_{cone}}{\left(2\frac{d\theta}{dx}\right)_{flat\ plate}}$$

for zero pressure gradient

$$c_{f_w} = \frac{\tau_o}{\frac{1}{2}\rho_w u_1^2}$$

C_F mean skin friction coefficient

$$= \frac{F}{\frac{1}{2}\rho_1 u_1^2 S} = \frac{\left(4\frac{\theta}{x}\right)_{cone}}{\left(2\frac{\theta}{x}\right)_{plate}}$$

for no pressure gradient

$$C_{F_w} = \frac{F}{\frac{1}{2}\rho_w u_1^2 S}$$

$$u_\tau = \left(\frac{\tau_o}{\rho_1}\right)^{\frac{1}{2}}$$

$$u_{\tau_w} = \left(\frac{\tau_o}{\rho_w}\right)^{\frac{1}{2}}$$

$$y_\tau = \frac{u_\tau y}{\nu_1}$$

$$y_{\tau_w} = \frac{u_{\tau_w} y}{\nu_w}$$

β temperature recovery factor $= \dfrac{T_{w_o} - T_1}{T_o - T_1}$

σ Prandtl No. $\left(\dfrac{\mu C_p}{k}\right)$

C_p specific heat of air at constant pressure

k thermal conductivity of air

Subscript w refers to conditions at wall temperature T_w

REFERENCES

No.	Author	Title, etc.
1	J.E. Johnson R.J. Monaghan	Measurement of heat transfer and skin friction at supersonic speeds: Preliminary results of measurements on a flat plate at Mach No. of 2.5. C.P.59. April 1949.
2	R.J. Monaghan J.E. Johnson	The measurement of heat transfer and skin friction at supersonic speeds. Part II. Boundary layer measurements on a flat plate at M = 2.5 and zero heat transfer. C.P.64. December 1949.
3	R.J. Monaghan J.R. Cooke	The measurement of heat transfer and skin friction at supersonic speeds. Part III. Measurements of overall heat transfer and of the associated boundary layers on a flat plate at M = 2.43. C.P.139. December 1951.
4	Hantzsche, W. Wendt, H.	The laminar boundary layer on a circular cone at zero incidence in a supersonic stream. MAP - Völkenrode - Refs: MAP - V487 (MOS 115). Reports and Translation No. 276. August 1946. ARC. 10,277.
5	K.W. Mangler	Boundary layers on bodies of revolution in symmetrical flow. MAP Völkenrode Ref: MAP - VG46 - 55T. Reports and Translation No. 55. April 15th, 1946.
6	-	Tables of supersonic flow around cones. Technical Report No. 1. NOrd Contract No. 9169. Massachusetts Institute of Technology. Cambridge, Massachusetts, 1947.
7	F.V. Davies	Some effects of pitot size on the measurement of boundary layers in supersonic flow. Tech Note Aero 2179. August 1952. ARC No. 15,430.
8	J.R. Cooke	The use of quartz in the manufacture of small diameter pitot tubes. Tech Note No. Aero 2325. 1954.
9	R.J. Monaghan	An approximate solution of the compressible laminar boundary layer on a flat plate. R.& M.2760. November 1949.
10	W.F. Cope G.G. Watson	Preliminary measurements of the boundary layer in the 11" supersonic wind tunnel. R.& M.2304. August 1946.

REFERENCES (Contd)

No.	Author	Title, etc.
11	H.B. Squire	Heat transfer calculation for aerofoils. R.& M. No. 1986. November 1942.
12	A.D. Young	The calculation of the profile drag of aerofoils and bodies of revolution at supersonic speeds. ARC No. 15,970. FM 1916. College of Aeronautics Report No.73. April 1953.
13	E.R. Van Driest	Turbulent boundary layer on a cone in a supersonic flow at zero angle of attack. Journal of the Aeronautical Sciences. Vol. 19. No.1. pp. 55. January 1952.
14	R.J. Monaghan	A survey and correlation of data on heat transfer by forced convection at supersonic speeds. Tech Note No. Aero 2259. September 1953. ARC No. 16,528.

APPENDIX I

The laminar boundary layer (approximate algebraic solutions[9])

The theoretical solution for the laminar boundary layer in this note is taken from ref.9. Simple approximate algebraic solutions are obtained by using the following relations for shear stress and temperature distributions and viscosity:

(a) Young's shear stress velocity relation

$$\frac{F}{F_o} = \sqrt{1 - \left(\frac{u}{u_1}\right)^2} \qquad (I.1)$$

where F_o the shear stress at the wall is defined by

$$F_o = c_f \sqrt{Re_x} \; ; \qquad (I.2)$$

(b) a temperature velocity relation

$$\frac{T}{T_1} = \frac{T_w}{T_1} - \sigma^{\frac{1}{3}} \frac{(T_w - T_{w_o})}{T_1} \left(\frac{u}{u_1}\right) - \sigma \frac{(\gamma - 1)}{2} M_1^2 \left(\frac{u}{u_1}\right)^2$$

$$= A - B\left(\frac{u}{u_1}\right) - D\left(\frac{u}{u_1}\right)^2 \; ; \qquad (I.3)$$

(c) a viscosity temperature relation

$$\frac{\mu}{\mu_1} = C \frac{T}{T_1}$$

C being a constant derived from the Sutherland formula to fit the variation of viscosity with temperature over the temperature range concerned.

From these relations the following analytic solutions of the laminar boundary layer integrals are obtained:

$$\delta^* = 2 \frac{C}{F_o} \frac{x}{\sqrt{Re_x}} \left\{ \left(A - \frac{D}{2}\right) \frac{\pi}{2} - (B + 1) \right\} \qquad (I.4)$$

$$\theta = 2 \frac{C}{F_o} \frac{x}{\sqrt{Re_x}} \left\{ \frac{4 - \pi}{4} \right\} \qquad (I.5)$$

$$H = \frac{\delta^*}{\theta} = \frac{4}{4 - \pi} \left\{ \left(A - \frac{D}{2}\right) \frac{\pi}{2} - (B + 1) \right\} \qquad (I.6)$$

$$\frac{1}{2} \frac{y}{x} \sqrt{Re_x} = \frac{C}{F_o} \left\{ \left(A - \frac{D}{2}\right) \sin^{-1} z + \left(\frac{Dz}{2} + B\right) \sqrt{1 - z^2} - B \right\} \qquad (I.7)$$

where

$$z = \frac{u}{u_1} \, .$$

For the boundary layer on a cone in a supersonic flow

$$F_o = \left(2\frac{d\theta}{dx} + 2\frac{\theta}{x}\right)\sqrt{Re_x}$$

$$= \sqrt{\frac{4-\pi}{2}}\sqrt{C}\sqrt{3} \qquad \text{from equation (I.5)}$$

$$= 0.655\sqrt{C}\sqrt{3} \qquad (I.8)$$

i.e. $$(F_o)_c = \sqrt{3}\,(F_o)_p .$$

Substituting for C in equation (I.5)

$$\theta = \frac{(F_o)_c}{3}\frac{x}{\sqrt{Re_x}} \qquad (I.9)$$

i.e. equations (I.5) and (I.9) are identical for the relation

$$F_o = 0.655\sqrt{C}\sqrt{3} .$$

However, in ref.2 Crocco's relation for a flat plate

$$F_o = 0.664\sqrt{C}$$

has been used and to allow comparison to be made with these results the corresponding value for a cone is used, i.e.

$$F_o = 0.664\sqrt{C}\sqrt{3} . \qquad (I.10)$$

Equations (I.5) and (I.9) are not consistent for Crocco's relation between F_o and C and it is necessary to define δ^* and θ as

$$\theta = \tfrac{1}{3}(F_o)_c\,(Re_x)^{-\frac{1}{2}}x \qquad (I.11)$$

$$\delta^* = H.\theta . \qquad (I.12)$$

A value for C can be determined so that equation (I.3) gives a good approximation to the Sutherland viscosity formula over the appropriate temperature range. A detailed derivation of the expression for C is given in ref.2 but only the results need be stated here, i.e.

$$C = \sqrt{\frac{T_1}{T'}}\,\frac{\left(1+\frac{T_o}{T_1}\right)}{\left(1+\frac{T_o}{T'}\right)} \qquad (I.13)$$

where $T_o = 116^{\circ}K$ and T' is a temperature intermediate between T_w and T_1 given by

$$\frac{T'}{T_1} = \frac{T_w}{T_1} - 0.468\,\sigma^{\frac{1}{3}}\frac{(T_w - T_{w_o})}{T_1} - 0.273\,\sigma\frac{(\gamma-1)}{2}M_1^2 . \qquad (I.14)$$

For zero heat transfer conditions

$$T_{w_o} = T_w$$

and the expressions for the constants become

$$A = \frac{T_{w_o}}{T_1} = \left\{1 + \sigma^{\frac{1}{2}} \frac{\gamma-1}{2}\right\} \tag{I.15}$$

$$B = 0$$

$$\frac{T'}{T_1} = \frac{T_{w_o}}{T_1} - 0.273\sigma \frac{(\gamma-1)}{2} M_1^2 \tag{I.16}$$

$$= \left\{1 + \frac{\gamma-1}{2} M_1^2 \left(\sigma^{\frac{1}{2}} - 0.273\sigma\right)\right\}$$

$$D = \sigma \frac{(\gamma-1)}{2} M_1^2 .$$

For $M_1 = 2.35$ these give

$$A = 1.938, \quad B = 0, \quad C = 0.936 \quad \text{and} \quad D = 0.796$$

which when substituted into equation (I.6), (I.7), (I.10), (I.11) and (I.12) give the laminar boundary layer equations used for comparison with experimental data:

$$\delta^* = 2.445 \, Re_x^{-\frac{1}{2}} \, x \tag{I.17}$$

$$\theta = 0.371 \, Re_x^{-\frac{1}{2}} \, x \tag{I.18}$$

$$H = 6.61 \tag{I.19}$$

$$\frac{y}{x}\sqrt{Re_x} = 1.682 \left\{1.54 \sin^{-1} z + 0.398 z \sqrt{1-z^2}\right\} . \tag{I.20}$$

For $M_1 = 2.23$

$$A = 1.846, \quad B = 0, \quad C = 0.936 \quad \text{and} \quad D = 0.716$$

giving

$$\delta^* = 2.30 \, (Re_x)^{-\frac{1}{2}} \, x \tag{I.21}$$

$$\theta = 0.371 \, (Re_x)^{-\frac{1}{2}} \, x \tag{I.22}$$

$$H = 6.22 \tag{I.23}$$

$$\frac{y}{x}\sqrt{Re_x} = 1.682 \left\{1.488 \sin^{-1} z + 0.358 z \sqrt{1-z^2}\right\} . \tag{I.24}$$

APPENDIX II

A comparison between turbulent boundary layers on a cone and flat plate based on a log law analysis (refs.13 and 2)

The analysis in this appendix is similar in form to that of Van Driest[13] but is based on the constancy of velocity profile advanced in ref.2. The relations obtained between the boundary layers on flat plates and cones are different from those of Van Driest, the differences being due to second order terms in the solution.

The assumption will be made that on both flat plates and cones the velocity profile in compressible flow is given by

$$\frac{u}{u_{\tau_w}} = D + \frac{1}{k} \log_e y_{\tau_w} \qquad (II.1)$$

where $u_{\tau_w} = \frac{\sqrt{\tau}}{\sqrt{\rho_w}}$ and $y_{\tau_w} = \frac{u_{\tau_w} y}{\nu_w}$

the subscript w referring to conditions at the surface.

Equation (II.1) can be written

$$y = \frac{a\, \nu_w\, s}{u_1} e^{ksz} \qquad (II.2)$$

and

$$dy = \frac{a\, k\, s^2\, \nu_w}{u_1} e^{ksz}\, dz \qquad (II.3)$$

where $s = \frac{u_1}{u_{\tau_w}} = \sqrt{\frac{2}{c_{f_w}}}$ and $z = \frac{u}{u_1}$.

The relation between the temperature and density profiles and the velocity profile is assumed to be

$$\frac{T}{T_w} = 1 - \beta z - \alpha z^2 = \frac{\rho_w}{\rho}. \qquad (II.4)$$

Equations (II.3) and (II.4) are substituted in the momentum equation

$$\rho_1\, u_1^2\, \theta = \int_0^\delta \rho u\, (u_1 - u)\, dy \qquad (II.5)$$

giving

$$\frac{u_1 \theta}{\nu_w} = \frac{T_1}{T_w}\, a\, k\, s^2 \int \frac{z(1-z)\, e^{ksz}\, dz}{(1 - \beta z - \alpha z^2)}. \qquad (II.6)$$

The solution of this integral (see ref.2) is

$$\frac{u_1 \theta}{\nu_w} = \frac{a}{k} e^{ks} \left\{ 1 + O\left(\frac{1}{s^2}\right) \right\}. \qquad (II.7)$$

Thus for s large

$$\frac{u_1 \theta}{\nu_w} = \frac{a}{k} e^{ks} \qquad (II.8)$$

for flat plates and cones.

(a) Flat plate

The skin friction equation

$$\frac{d\theta}{dx} = \frac{c_f}{2} = \frac{1}{s^2} \frac{T_1}{T_w} . \qquad (II.9)$$

Now from equation (II.8)

$$\frac{u_1}{\nu_w} \frac{d\theta}{dx} = \frac{a}{k} \frac{d\,(e^{ks})}{dx} \qquad (II.10)$$

and

$$\frac{u_1 x}{\nu_w} \frac{T_1}{T_w} = \frac{a}{k} \int s^2 \, d\,(e^{ks}) . \qquad (II.11)$$

Integrating, this becomes

$$\frac{u_1 x}{\nu_w} = \frac{T_w}{T_1} \frac{a\, s^2}{k} e^{ks} \left[1 - 2 \left(\frac{1}{ks} - \frac{1}{k^2 s^2} \right) \right]$$

$$= \frac{T_w}{T_1} \frac{as^2}{k} e^{ks} \left[1 - \frac{2}{ks} \right] \qquad (II.12)$$

ignoring the second order term.

(b) Cone

The skin friction equation

$$\frac{d\theta}{dx} + \frac{\theta}{x} = \frac{1}{s^2} \frac{T_1}{T_w} \qquad (II.13)$$

may be written

$$\frac{d\,(\theta x)}{dx} = \frac{x}{s^2} \frac{T_1}{T_w} \qquad (II.14)$$

and from equation (II.8)

$$\frac{u_1\, \theta x}{\nu_w} = \frac{ax}{k} e^{ks} \qquad (II.15)$$

and

$$\frac{u_1}{\nu_w} \frac{d\,(\theta x)}{dx} = \frac{a}{k} \frac{d}{dx} (x\, e^{ks}). \qquad (II.16)$$

Thus
$$\frac{u_1}{\nu_w} x = \frac{a s^2}{k} \frac{T_w}{T_1} \frac{d}{dx} (x e^{ks}) . \qquad (II.17)$$

Integrating
$$\frac{u_1 x^2}{2\nu_w} = \frac{a}{k} \frac{T_w}{T_1} \left[s^2 e^{ks} x - 2 \int x e^{ks} s \, ds \right] . \qquad (II.18)$$

Thus for s large x is given to a first order by

$$\frac{u_1 x_1}{2\nu_w} = \frac{a}{k} \frac{T_w}{T_1} s^2 e^{ks} \qquad (II.19)$$

$$\int x e^{ks} s \, ds = \frac{a}{k} \frac{T_w}{T_1} \frac{2\nu_w}{u_1} \int s^3 e^{2ks} \, ds$$

$$= \frac{s^2 e^{2ks}}{k^2} a \left\{ s - \frac{3}{2k} + \frac{3}{2k^2} \frac{1}{s} - \frac{3}{4k^3 s^2} \right\} \frac{\nu_w}{u_1} \frac{T_w}{T_1}$$

$$= \frac{x_1}{2k} e^{ks} \left\{ s - \frac{3}{2k} + 0 \left(\frac{1}{s} \right) \cdots \right\} .$$

Substituting in equation (II.18) x is given to a second order

$$\frac{u_1 x_2^2}{2\nu_w} = \frac{a}{k} \frac{T_w}{T_1} x_1 s^2 e^{ks} \left[1 - \left\{ \frac{1}{ks} - \frac{3}{2ks^2} + 0 \left(\frac{1}{s^3} \right) \cdots \right\} \right] \qquad (II.20)$$

and from equation (II.19)

$$\left(\frac{x_2}{x_1} \right)^2 = 1 - \frac{1}{ks} + 0 \left(\frac{1}{s^2} \right) .$$

Ignoring second order terms

$$\frac{x_2}{x_1} = \sqrt{1 - \frac{1}{ks}} .$$

Thus to a second order

$$\frac{u_1 x}{2\nu_w} = \frac{T_w}{T_1} \frac{a}{k} s^2 e^{ks} \sqrt{1 - \frac{1}{ks}} . \qquad (II.21)$$

Comparing this equation with the corresponding one (equation (II.12)) for the flat plate and assuming that the skin friction coefficient c_f and the heat transfer parameter T_w/T_1 are the same then

$$\frac{(Re_x)_c}{(Re_x)_p} = \frac{2\sqrt{1 - \frac{1}{ks}}}{\left(1 - \frac{2}{ks}\right)}$$

$$= 2\left\{1 + \frac{3}{2}\frac{1}{ks}\right\} \qquad \text{(II.22)}$$

for large values of s.

If the skin friction coefficient c_f is represented by a power law formula then

$$\frac{c_{f_c}}{c_{f_p}} = A \frac{(Re_x)_c^{-1/5}}{(Re_x)_p^{-1/5}} . \qquad \text{(II.23)}$$

Then for the same skin friction coefficients

$$A = \frac{(Re_x)_c^{1/5}}{(Re_x)_p^{1/5}} = \left\{2\left(1 + \frac{3}{2}\frac{1}{ks}\right)\right\}^{1/5}$$

and thus for the same Reynolds number

$$\frac{c_{f_c}}{c_{f_p}} = \left\{2\left(1 + \frac{3}{2}\frac{1}{ks}\right)\right\}^{1/5} . \qquad \text{(II.24)}$$

From equations (II.8), (II.12) and (II.21)

$$\frac{(Re_x)_c}{(Re_x)_p} = \frac{\theta_c}{\theta_p}\frac{s_c^2}{s_p^2}\left\{2\left(1 + \frac{3}{2}\frac{1}{ks}\right)\right\}$$

$$= \frac{\theta_c}{\theta_p}\frac{c_{f_p}}{c_{f_c}}\left\{2\left(1 + \frac{3}{2}\frac{1}{ks}\right)\right\}$$

and for the same Reynolds number

$$\frac{\theta_c}{\theta_p} = \left\{2\left(1 + \frac{3}{2}\frac{1}{ks}\right)\right\}^{-4/5} \qquad \text{(II.25)}$$

and since

$$\frac{(C_F)_c}{(C_F)_p} = \frac{2\theta_c}{\theta_p}$$

$$= 2\left\{2\left(1 + \frac{3}{2}\frac{1}{ks}\right)\right\}^{-4/5} . \qquad \text{(II.26)}$$

Some results taken from equations (II.22), (II.24), (II.25) and (II.26) are tabulated below. Values of corresponding skin friction coefficients are taken from the flat plate formula[14]

$$\frac{c_{f_w}}{2} = \frac{1}{s^2} = 0.0296 \left(Re_w \frac{T_1}{T_w} \right)^{-1/5} . \qquad (II.27)$$

The Reynolds number $\left(Re_w \frac{T_1}{T_w} = \frac{u_1 x}{\nu_w} \frac{T_1}{T_w} \right)$ is a significant parameter for the cone flat plate relations, but corresponding values of $\left(Re_x = \frac{u_1 x}{\nu_1} \right)$ for a Mach number of 2.35 and zero heat transfer conditions are included in the table for general comparison. The parameters marked thus * are for equal cone and flat plate skin friction coefficients; those marked ** are for equal cone and flat plate Reynolds numbers.

$Re_w \frac{T_1}{T_w}$	10^5	10^6	10^7
Re_x	6.4×10^5	6.4×10^6	6.4×10^7
$\frac{c_{f_w}}{2} = \frac{1}{s^2}$	0.00296	0.00187	0.00118
* $\frac{(Re_x)_c}{(Re_x)_p}$	2.408	2.324	2.258
** $\frac{c_{f_c}}{c_{f_p}}$	1.192	1.184	1.177
** $\frac{\theta_c}{\theta_p}$	$\frac{1}{2.025}$	$\frac{1}{1.962}$	$\frac{1}{1.917}$
** $\frac{C_{F_c}}{C_{F_p}}$	0.988	1.019	1.043

APPENDIX III

A summary of Young's correlation[12] between the turbulent boundary layers for 2 dimensional and axi-symmetric flow extended to the cone-flat plate case

Young assumes the skin friction for both two dimensional and axi-symmetric flow to be given by

$$\frac{\tau_o}{\rho_1 u_1^2} = C\left(\frac{u_1 \theta}{\nu_1}\right)^{-\frac{1}{n-1}} h(M_1) \qquad \text{(III.1)}$$

C and n being constants identical for both cases. The compressibility functions $h(M_1)$ are likewise assumed to be identical for two dimensional and axi-symmetric flow in the analysis below.

The momentum equations for two dimensional and axi-symmetric flow are respectively

$$\frac{\partial \theta}{\partial x} + \theta\left[(H+2)\frac{1}{u_1}\frac{\partial u_1}{\partial x} + \frac{1}{\rho_1}\frac{\partial \rho_1}{\partial x}\right] = \frac{\tau_o}{\rho_1 u_1^2} \qquad \text{(III.2)}$$

$$\frac{\partial \theta}{\partial x} + \theta\left[(H+2)\frac{1}{u_1}\frac{\partial u_1}{\partial x} + \frac{1}{\rho_1}\frac{\partial \rho_1}{\partial x} + \frac{1}{r_o}\frac{\partial r_o}{\partial x}\right] = \frac{\tau_o}{\rho_1 u_1^2} \qquad \text{(III.3)}$$

where r_o is the radius of the axi-symmetric body.

The solutions to these equations are obtained by substituting for $\frac{\tau_o}{\rho_1 u_1^2}$: θ and $\frac{\tau_o}{\rho_1 u_1^2}$ can then be obtained in terms of x. In their most general form these solutions involve integrals of flow and body shape parameters. If as in the cases considered in this note the two dimensional flow is uniform flow over a flat plate and the axi-symmetric flow is supersonic flow over a cone then the momentum equations simplify and the complexity of the solutions is correspondingly reduced. Thus for a flat plate in a uniform flow equation (III.2) becomes

$$\frac{d\theta_p}{dx} = \frac{\tau_o}{\rho_1 u_1^2} = C\left(\frac{u_1 \theta_p}{\nu_1}\right)^{-\frac{1}{n-1}} h(M) \qquad \text{(III.4)}$$

and for a cone

$$\frac{d\theta_c}{dx} + \frac{\theta_c}{x} = \frac{\tau_o}{\rho_1 u_1^2} = C\left(\frac{u_1 \theta_c}{\nu_1}\right)^{-\frac{1}{n-1}} h(M) \, . \qquad \text{(III.5)}$$

The latter can be written

$$\frac{d\,(\theta_c x)}{dx} = C\left(\frac{u_1}{\nu_1}\right)^{-\frac{1}{n-1}} h(M)\,(x\,\theta_c)^{-\frac{1}{n-1}}\, x^{\frac{n}{n-1}} . \qquad \text{(III.6)}$$

Assuming that the boundary layer is turbulent from the leading edge or tip of the body and that $h(M)$ is not a function of x then equations (III.4) and (III.6) can be integrated to give

$$\theta_p^{\frac{n}{n-1}} = \frac{n}{n-1} C\left(\frac{u_1}{\nu_1}\right)^{-\frac{1}{n-1}} h(M)\, x \qquad \text{(III.7)}$$

$$\theta_c^{\frac{n}{n-1}} = \frac{n}{2n-1} C\left(\frac{u_1}{\nu_1}\right)^{-\frac{1}{n-1}} h(M)\, x \qquad \text{(III.8)}$$

respectively.

Thus

$$\frac{\theta_c}{\theta_p} = \left[\frac{n-1}{2n-1}\right]^{\frac{n-1}{n}} . \qquad \text{(III.9)}$$

The value of n corresponding to the $1/7$th power law is $n = 5$ which gives

$$\frac{\theta_c}{\theta_p} = \frac{1}{1.91} .$$

The relations for skin friction follow

$$\frac{c_{f_c}}{c_{f_p}} = \left[\frac{2n-1}{n-1}\right]^{\frac{1}{n}}$$

$$= 1.176 \quad \text{for} \quad n = 5$$

and

$$\frac{C_{F_c}}{C_{F_p}} = 2\left[\frac{n-1}{2n-1}\right]^{\frac{n-1}{n}}$$

$$= 1.045 \quad \text{for} \quad n = 5 .$$

These expressions are relatively insensitive to the value of n used within the normal range of n. That is, values of $n = 4$ and $n = 6$ corresponding to $1/5$th and $1/9$th power laws give a variation of θ_c/θ_p of $\pm$ 2 per cent from the value given for $n = 5$.

APPENDIX IV

Some empirical relations between the turbulent boundary layer characteristics for flow over cones and flat plates

The following transformation equations (analogous to the theoretical laminar boundary layer transformations of Hantzsche and Wendt[4], and Mangler[5]) between the displacement and momentum thicknesses functions for the turbulent boundary layers on cones and flat plates are used to compare with corresponding functions obtained from experimental data:

$$\frac{\{\delta^{*}(Re_X)^{1/n}\}_c}{\{\delta^{*}(Re_X)^{1/n}\}_p} = \text{const } B \qquad \text{(IV.1)}$$

and

$$\frac{\{\theta(Re_X)^{1/n}\}_c}{\{\theta(Re_X)^{1/n}\}_p} = B \quad . \qquad \text{(IV.2)}$$

where subscripts c and p refer to cone and flat plate respectively.

The subsequent transformations follow: If the momentum thickness on a flat plate can be represented by

$$\theta_p = A\,(Re_X)^{-1/n}\,X$$

then

$$\theta_c = B.A\,(Re_X)^{-1/n}\,X\,.$$

The local skin friction coefficients are

$$(c_f)_p = \frac{2d\theta_p}{dX} = \frac{2(n-1)}{n} A\,(Re_X)^{-1/n} \qquad \text{(IV.3)}$$

$$(c_f)_c = 2\left\{\frac{d\theta_c}{dX} + \frac{\theta_c}{X}\right\}$$

$$= 2BA\left\{\frac{2n-1}{n}\right\}(Re_X)^{-1/n}. \qquad \text{(IV.4)}$$

Then

$$\frac{[c_f\,Re_X^{1/n}]_c}{[c_f\,Re_X^{1/n}]_p} = \frac{B(2n-1)}{n-1}\,. \qquad \text{(IV.5)}$$

Similarly for the overall skin friction coefficients

$$(C_F)_p = \frac{2\theta_p}{X} = 2A\,(Re_X)^{-1/n} \qquad \text{(IV.6)}$$

$$(C_F)_c = \frac{4\theta_c}{X} = 4BA\,(Re_X)^{-1/n} \qquad (IV.7)$$

Then
$$\frac{(C_F\,Re_X^{1/n})_c}{(C_F\,Re_X^{1/n})_p} = 2B\,. \qquad (IV.8)$$

If the $^1/_7$th power law velocity profile is accepted (i.e. $n = 5$) and the factor B assumed to be $\frac{1}{\sqrt{3}}$ as in the laminar boundary layer case, then equations (IV.5) and (IV.8) become respectively

$$\frac{[c_f\,Re_X^{1/5}]_c}{[c_f\,Re_X^{1/5}]_p} = \tfrac{3}{4}\sqrt{3} \qquad (IV.9)$$

$$\frac{[C_F\,Re_X^{1/5}]_c}{[C_F\,Re_X^{1/5}]_p} = \frac{2}{3}\sqrt{3}\,. \qquad (IV.10)$$

APPENDIX V

Corrections to the experimental data due to differences in Mach number between the cones and flat plate

To obtain correspondence between the boundary layers on the cones and flat plate it is necessary to account for the effect of the Mach number M_1 (immediately outside the boundary layer) on the boundary layer functions (flat plate $M_1 = 2.45$, 10° cone $M_1 = 2.35$ and 20° cone $M_1 = 2.23$).

The corrections are set out below:

(a) Laminar boundary layer

The theoretical boundary layer functions for the flat plate[9] and the cones (Appendix I) show that

$$\frac{\theta_\alpha}{\theta_\beta} = \frac{(F_o)_\alpha}{(F_o)_\beta} = \sqrt{\frac{(C)_\alpha}{(C)_\beta}} \qquad (V.1)$$

$$\frac{H_\alpha}{H_\beta} = \frac{\left\{\left(A - \frac{D}{2}\right)\frac{\pi}{2} - B + 1\right\}_\alpha}{\left\{\left(A - \frac{D}{2}\right)\frac{\pi}{2} - B + 1\right\}_\beta} \qquad (V.2)$$

$$\frac{\delta^\times_\alpha}{\delta^\times_\beta} = \frac{(H.\theta)_\alpha}{(H.\theta)_\beta} \qquad (V.3)$$

where α and β refer to different values of M_1; A, B, C and D being functions of M_1.

Substituting the values of M_1 appropriate to the cones and flat plate, the following correction factors are obtained:

$$\frac{(\theta)_{M_1 = 2.35}}{(\theta)_{M_1 = 2.45}} = \frac{(\theta)_{M_1 = 2.23}}{(\theta)_{M_1 = 2.45}} = 1.00$$

$$\frac{(H)_{M_1 = 2.35}}{(H)_{M_1 = 2.45}} = \frac{(\delta^\times)_{M_1 = 2.35}}{(\delta^\times)_{M_1 = 2.45}} = \frac{1}{1.056}$$

$$\frac{(H)_{M_1 = 2.23}}{(H)_{M_1 = 2.45}} = \frac{(\delta^\times)_{M_1 = 2.23}}{(\delta^\times)_{M_1 = 2.45}} = \frac{1}{1.12} .$$

(b) Turbulent boundary layer

Assume that the boundary layer functions may be expressed as follows[3]:

$$C_F = A\,(Re_x)^{-1/5}\left(\frac{T_1}{T_w}\right)^{\frac{2.2}{5}} \tag{V.4}$$

$$\theta = B\,(Re_x)^{-1/5}\,x\left(\frac{T_1}{T_w}\right)^{\frac{2.2}{5}} \tag{V.5}$$

$$\frac{H}{H_i} = \frac{T_w}{T_1} + \frac{1}{5}M_1^2 \tag{V.6}$$

where A and B are constants.

For zero heat transfer

$$T_w = T_{w_o} = T_1\left\{1 + \sigma^{\frac{1}{3}}\frac{\gamma-1}{2}M_1^2\right\}$$

and equations (V.4), (V.5) and (V.6) become

$$C_F = A\,(Re_x)^{-1/5}\left\{1 + \sigma^{\frac{1}{3}}\frac{\gamma-1}{2}M_1^2\right\}^{-\frac{2.2}{5}} \tag{V.7}$$

$$\theta = B\,(Re_x)^{-1/5}\,x\left\{1 + \sigma^{\frac{1}{3}}\frac{\gamma-1}{2}M_1^2\right\}^{-\frac{2.2}{5}} \tag{V.8}$$

$$\frac{H}{H_i} = \left\{1 + M_1^2\left(\frac{1}{5} + \sigma^{\frac{1}{3}}\frac{\gamma-1}{2}\right)\right\}. \tag{V.9}$$

Thus for $M_1 = 2.45$ (flat plate) and $M_1 = 2.35$ (10° cone)

$$\frac{(C_F)_{M_1=2.35}}{(C_F)_{M_1=2.45}} = \frac{(\theta)_{M_1=2.35}}{(\theta)_{M_1=2.45}} = 1.02$$

$$\frac{(H)_{M_1=2.35}}{(H)_{M_1=2.45}} = \frac{1}{1.06}$$

$$\frac{(\delta^x)_{M_1=2.35}}{(\delta^x)_{M_1=2.45}} = \frac{1}{1.04}$$

To enable a comparison to be made between the various sets of experimental results solely on a basis of body geometry, all results in Tables I and II have, therefore, where necessary, been corrected to a Mach number of 2.35.

WT.2078.CP.284.K3 - Printed in Great Britain.

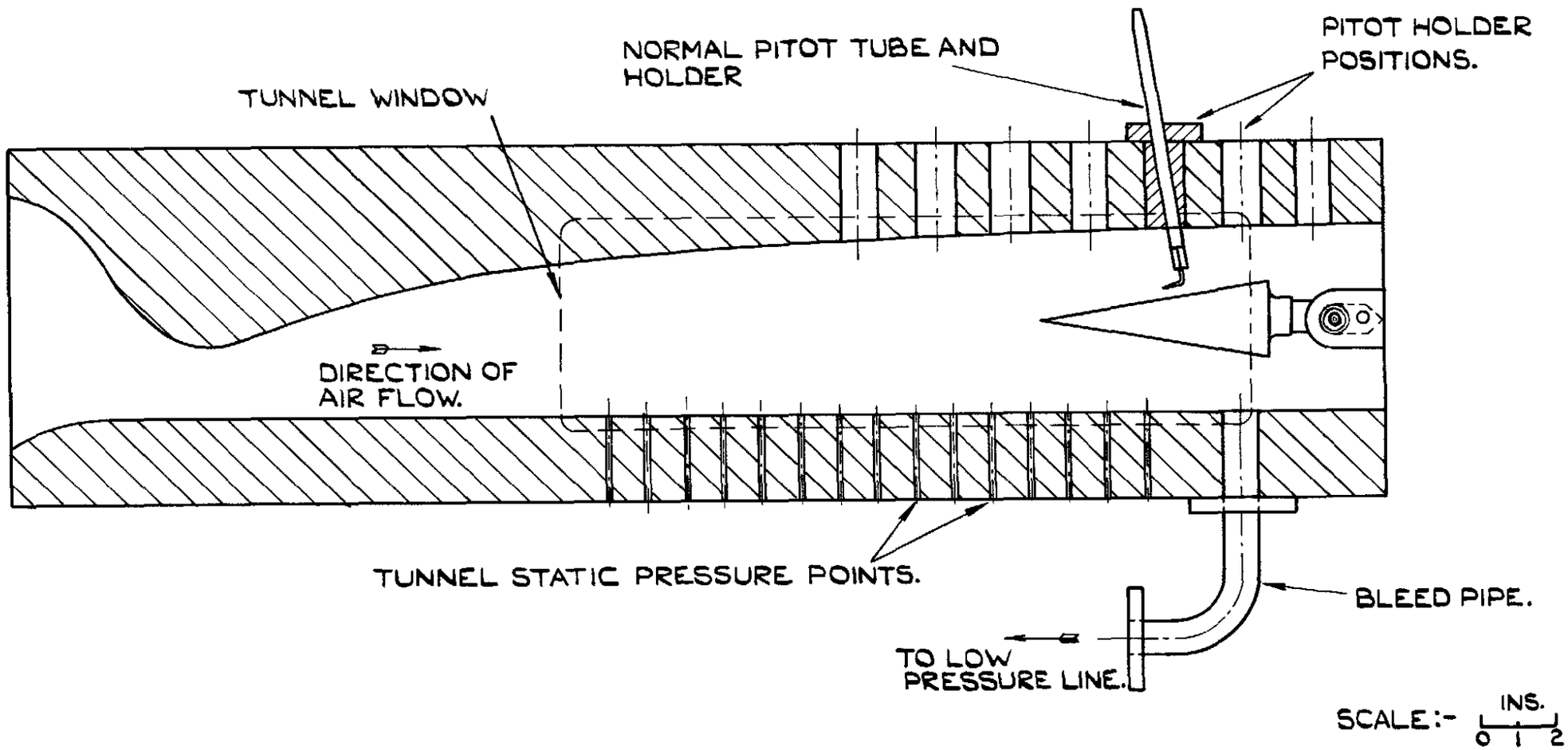

FIG. 1. TUNNEL WORKING SECTION SHOWING 20° CONE IN POSITION.

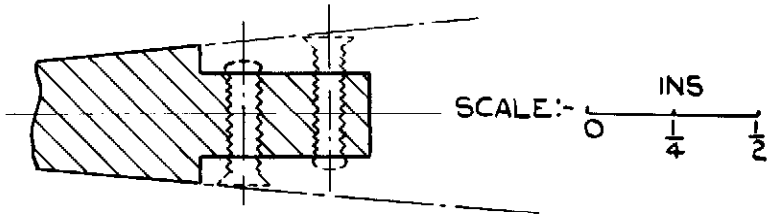

PART SECTION SHOWING NOSE FIXING.

PRESSURE POINTS - P
THERMOCOUPLES - T

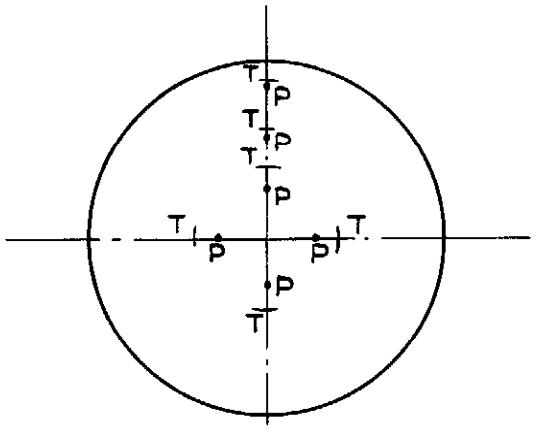

VIEW IN DIRECTION A-A

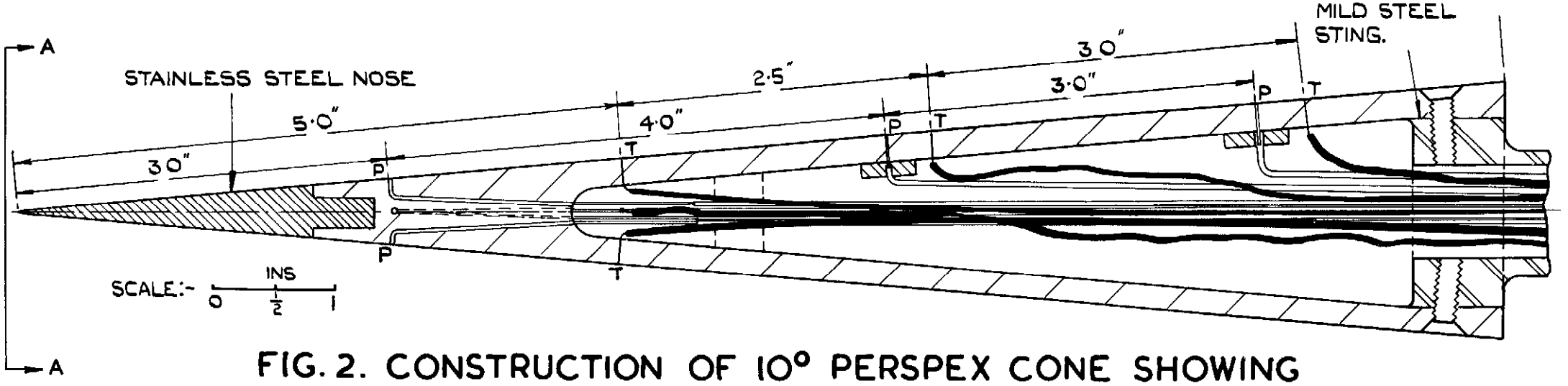

FIG. 2. CONSTRUCTION OF 10° PERSPEX CONE SHOWING THERMOCOUPLE & PRESSURE POINTS.

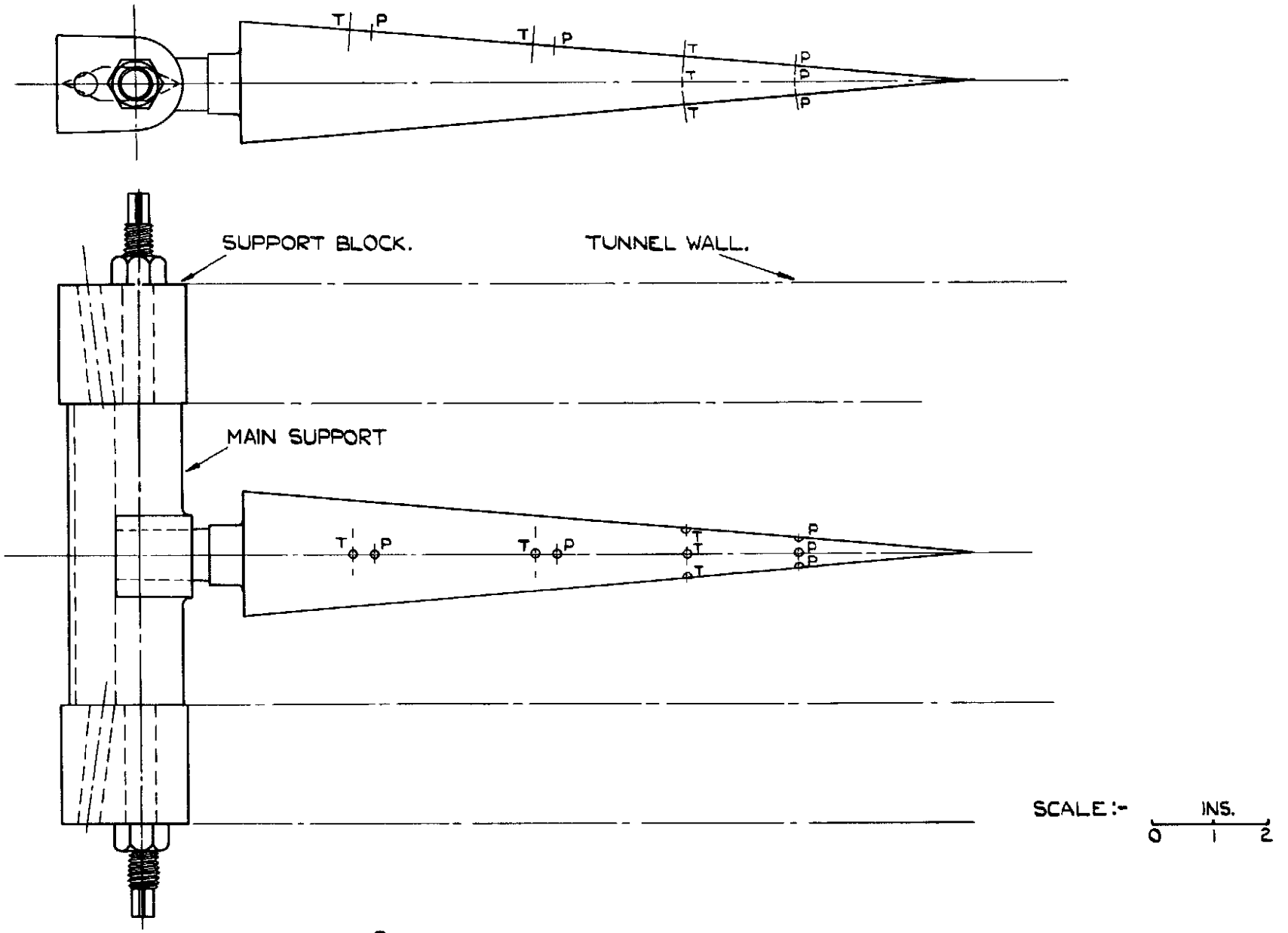

FIG. 3. 10° CONE & SUPPORT.

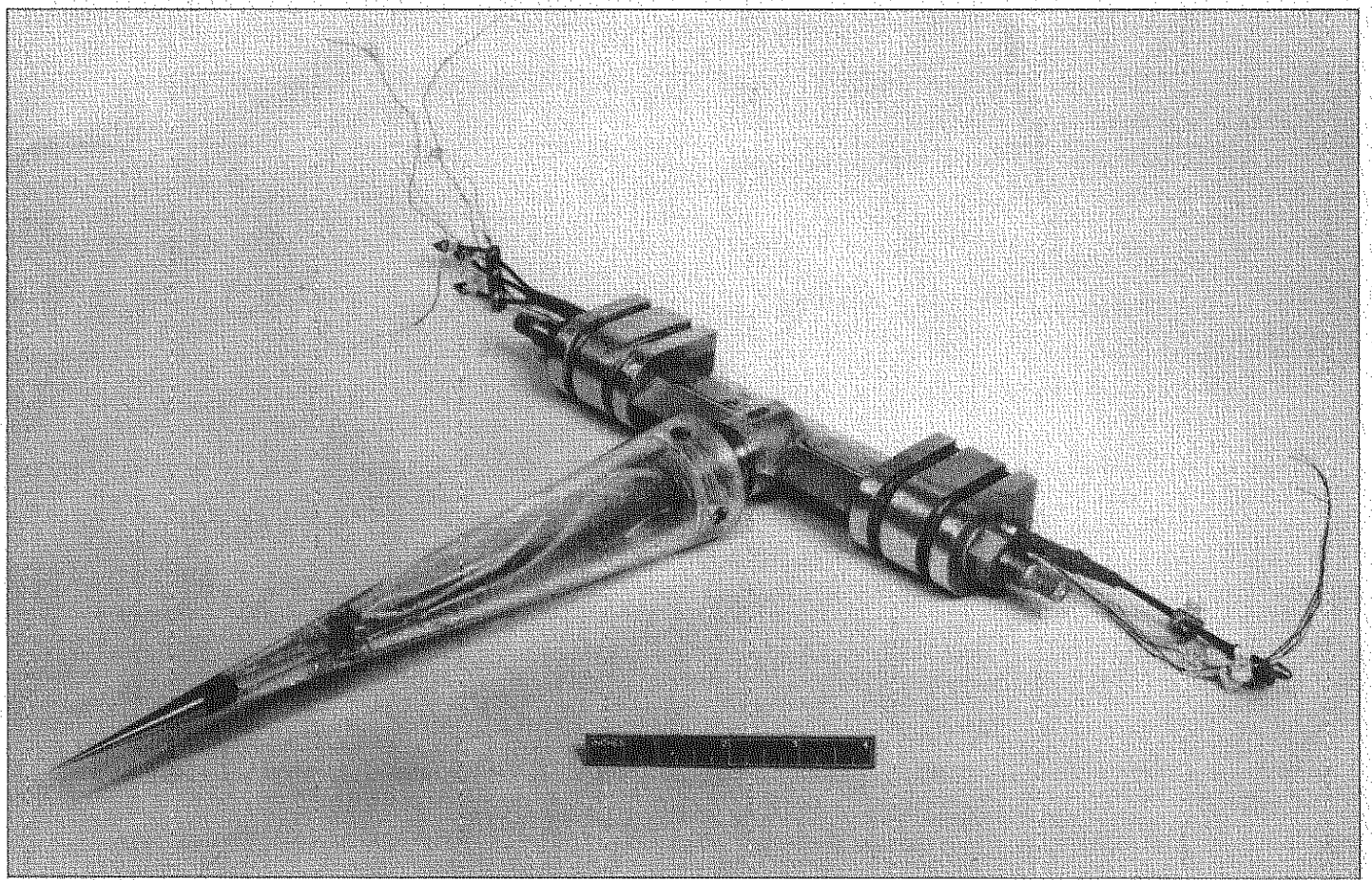

FIG.4. 10° PERSPEX CONE AND SUPPORTS

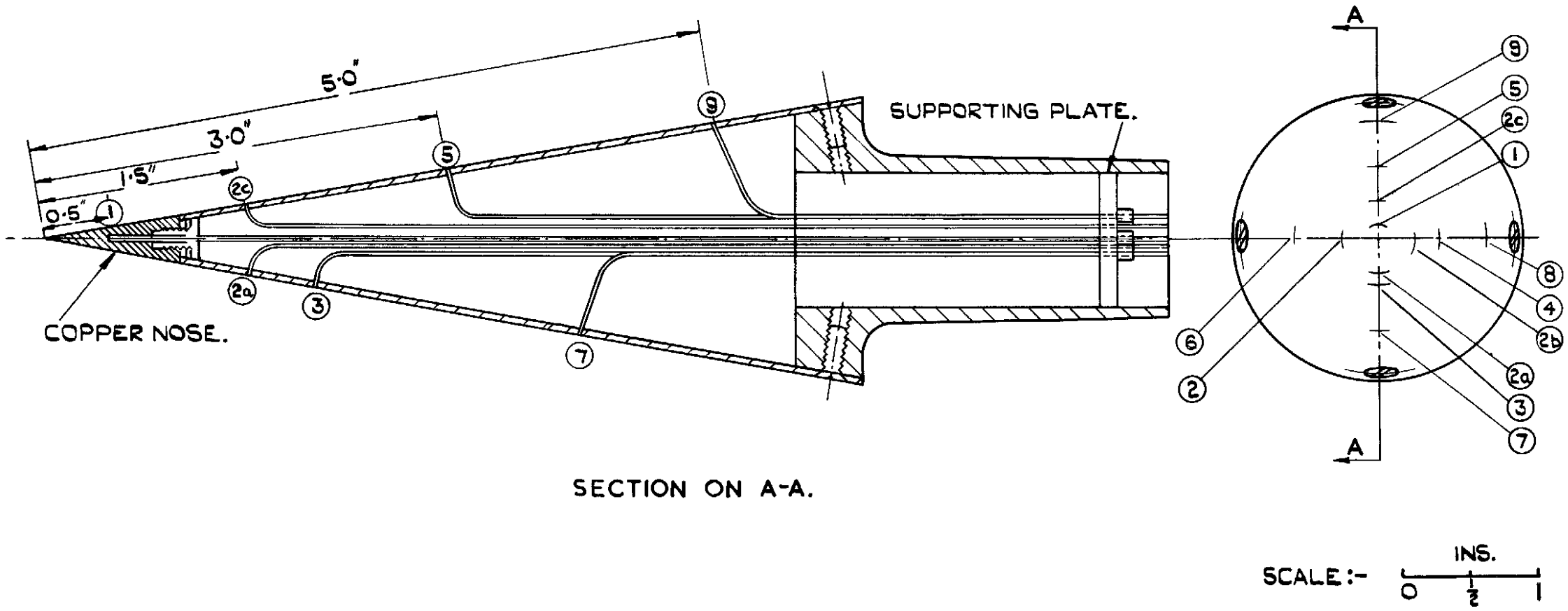

FIG. 5. 20° COPPER CONE SHOWING PRESSURE POINTS.

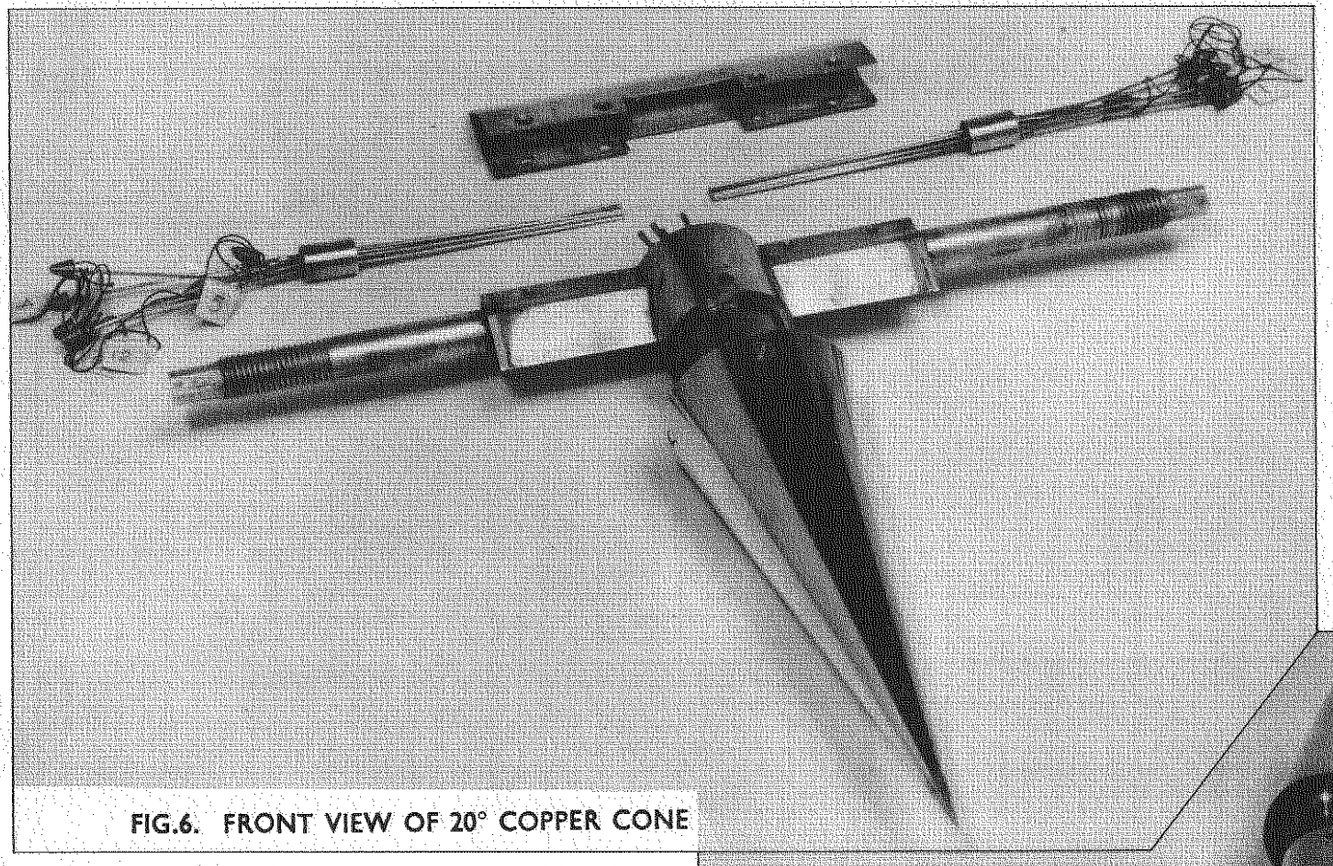

FIG.6. FRONT VIEW OF 20° COPPER CONE

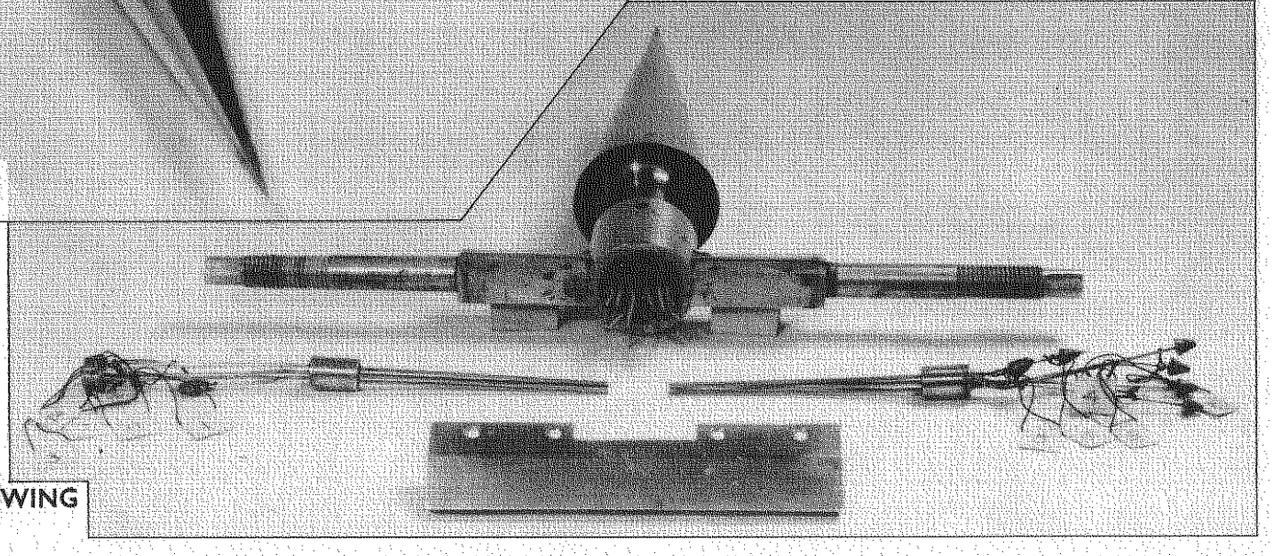

FIG.7. REAR VIEW OF 20° COPPER CONE SHOWING PRESSURE POINT CONNECTIONS

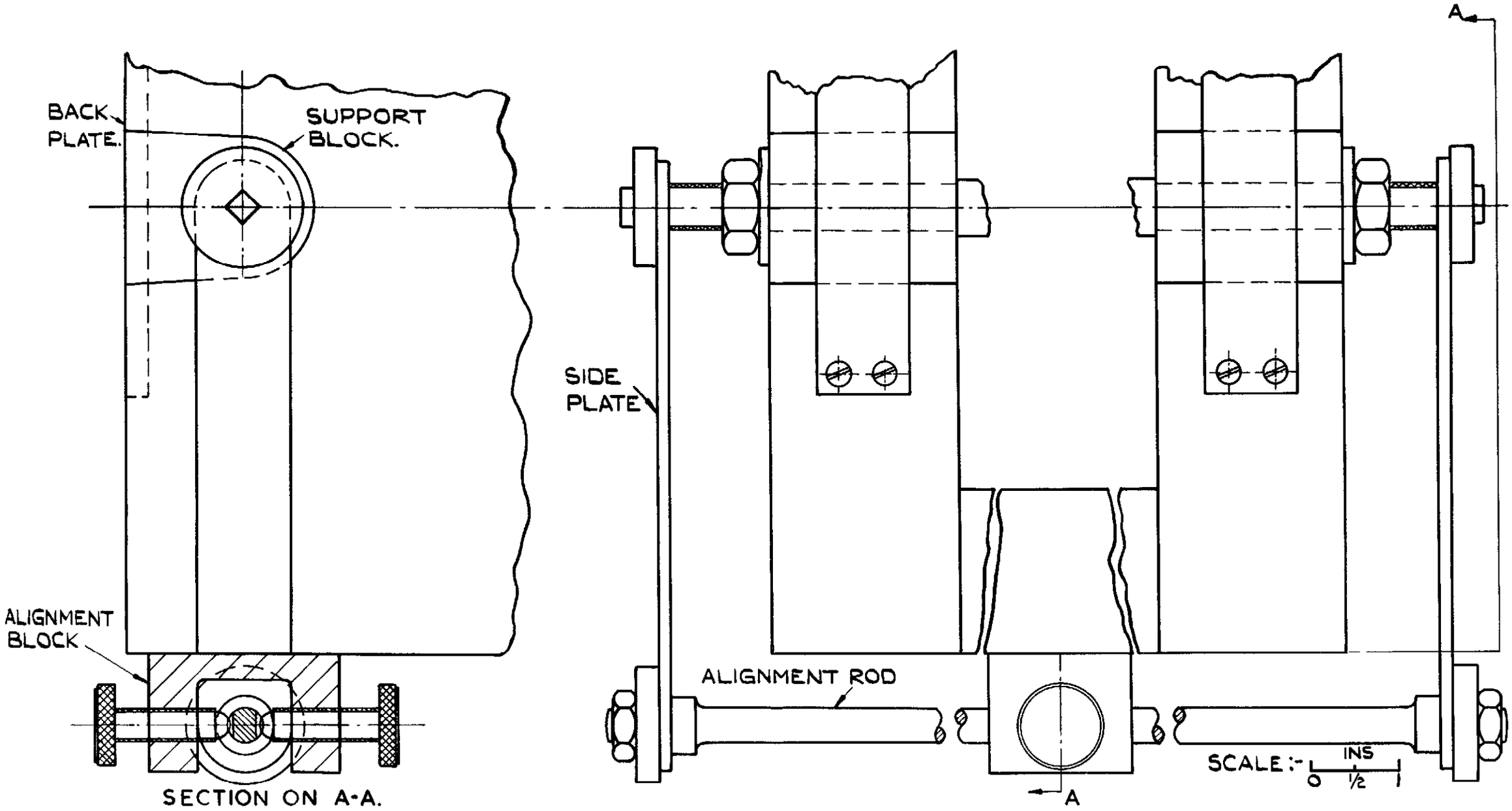

FIG.8. ARRANGEMENT OF SUPPORT BLOCKS IN TUNNEL SHOWING METHOD OF ALIGNMENT.

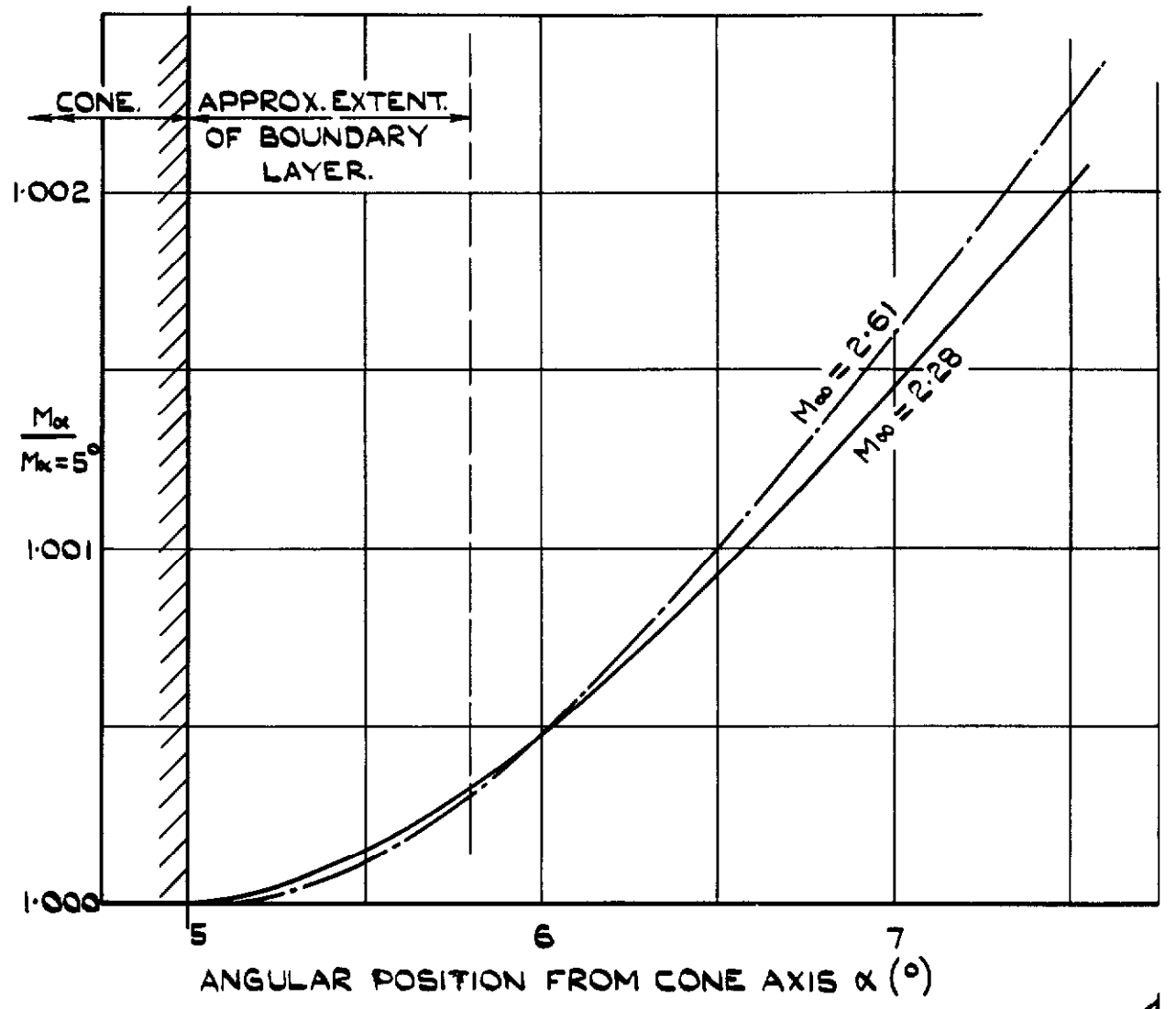

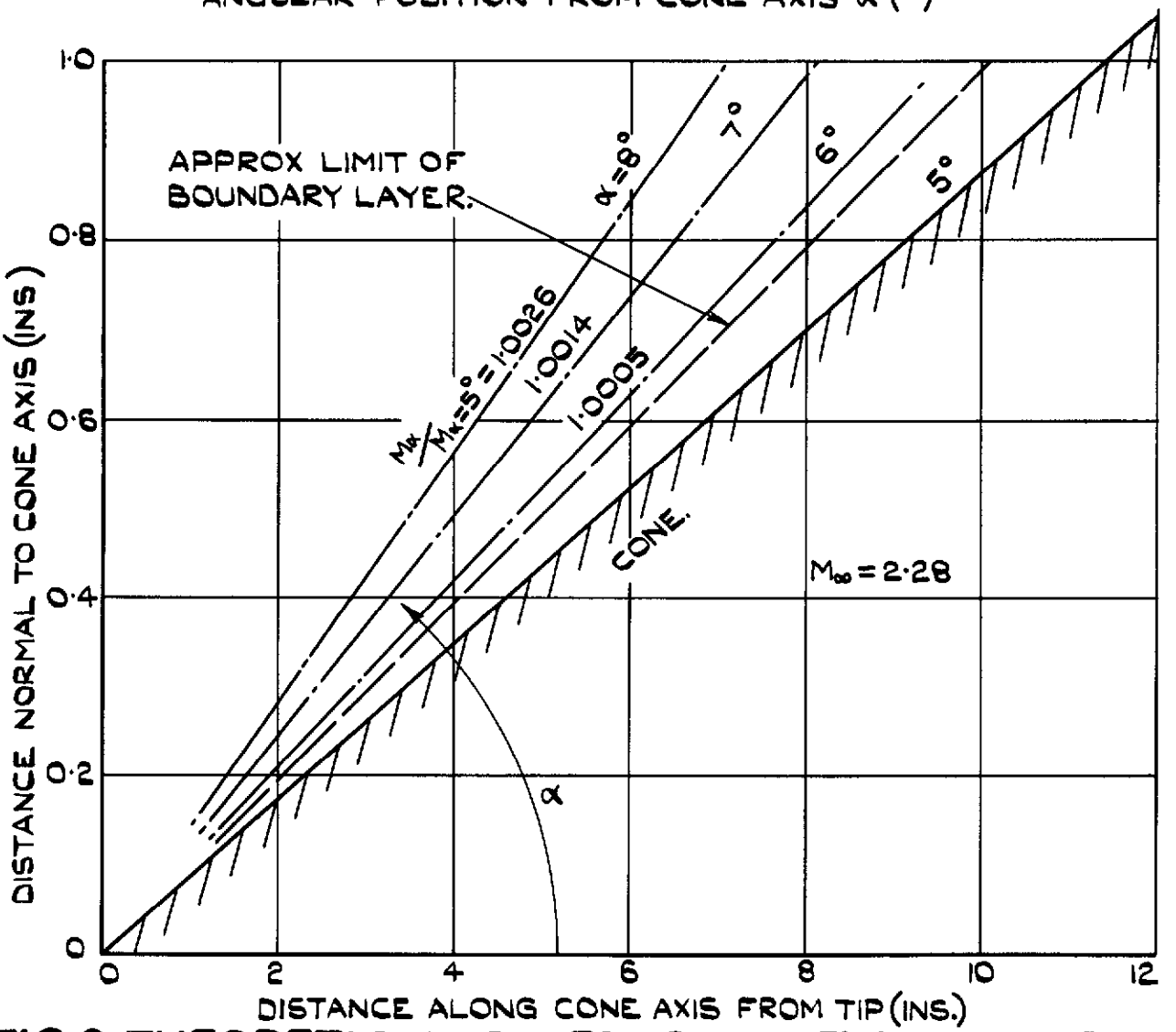

FIG. 9. THEORETICAL SUPERSONIC FLOW FIELD AROUND A CONE OF 10° TOTAL ANGLE.

$\left(M_\infty = \frac{2{\cdot}61}{2{\cdot}28}\right)$

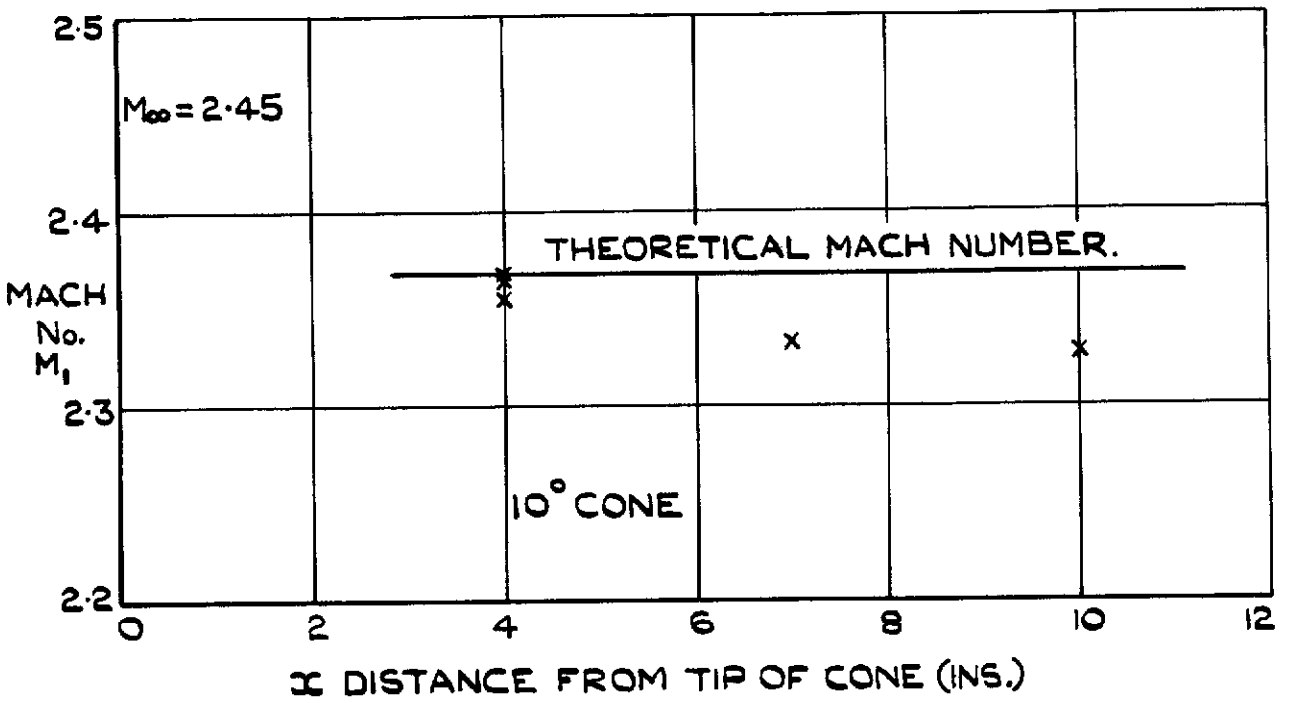

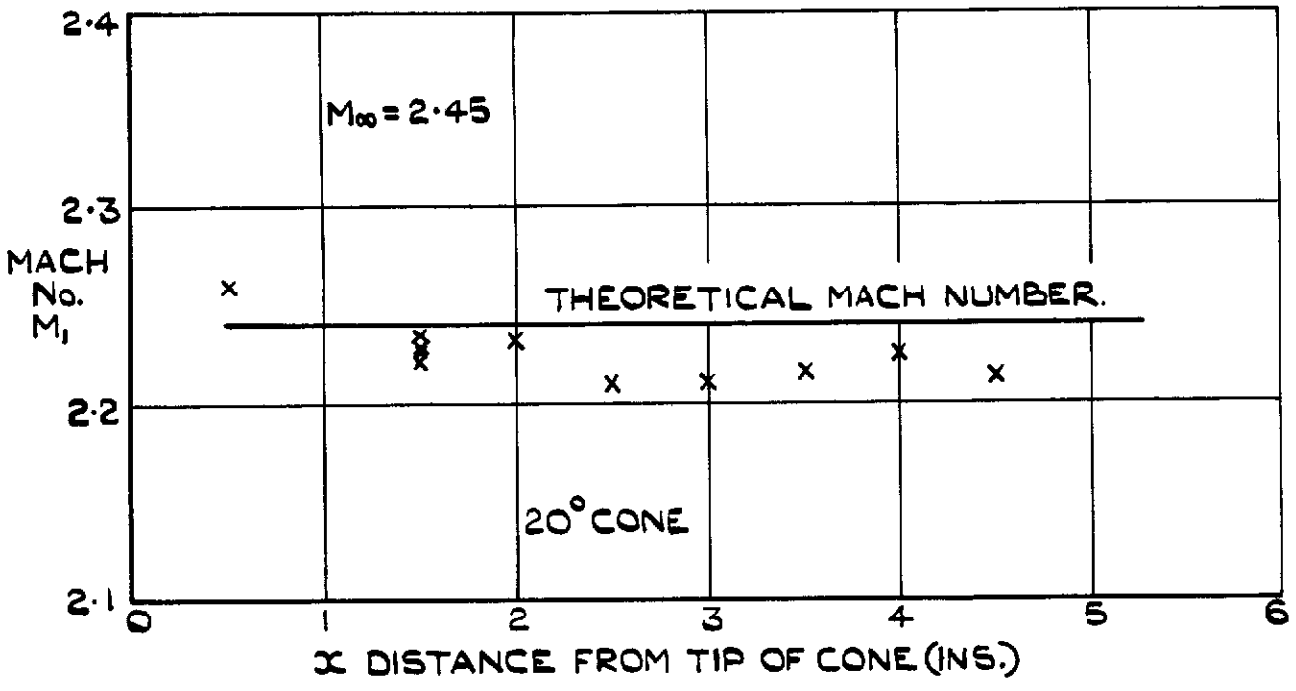

FIG. 10. MACH No. DISTRIBUTION ALONG CONES (FROM MEASURED STATIC PRESSURES ON CONE SURFACE.)

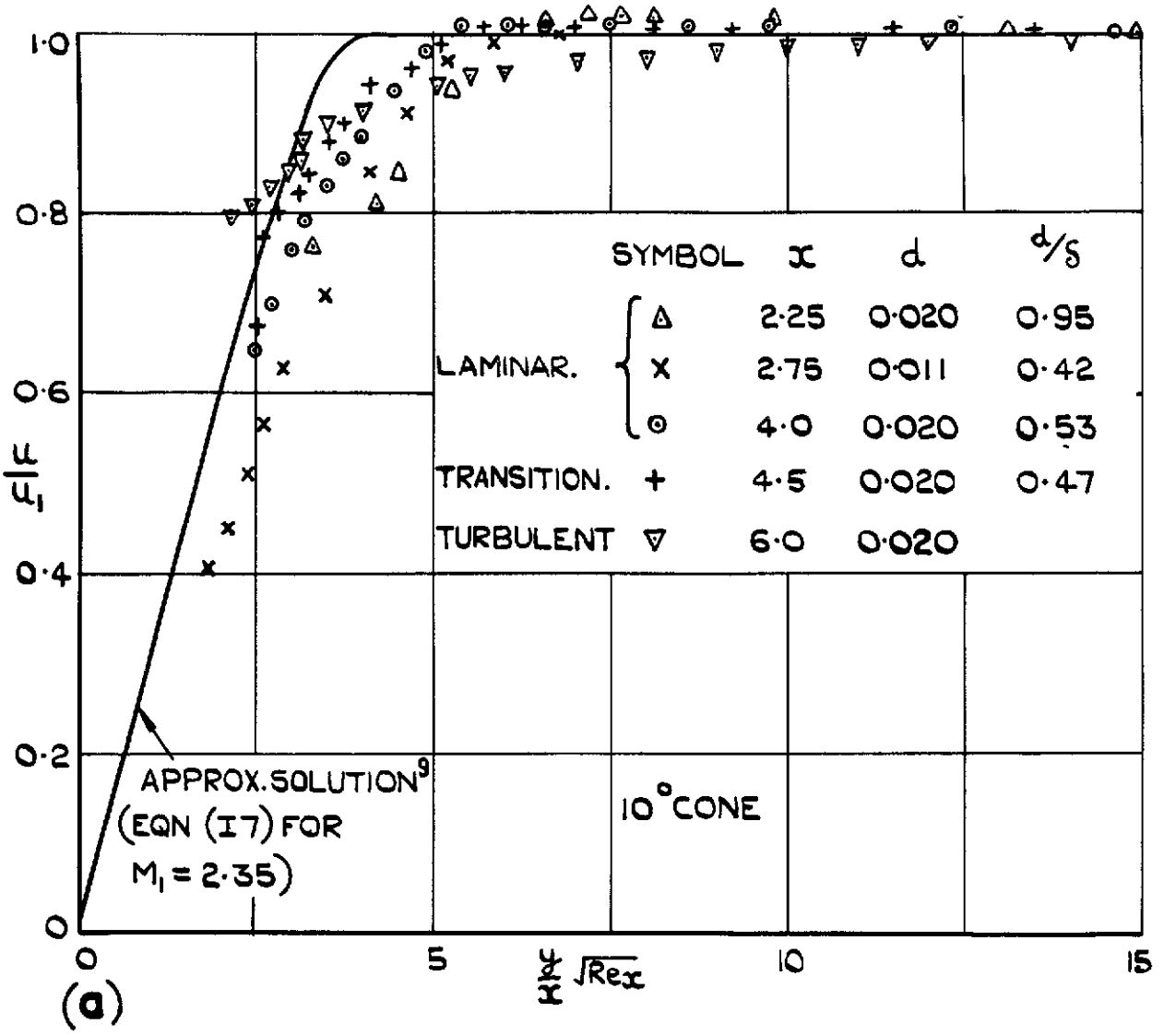

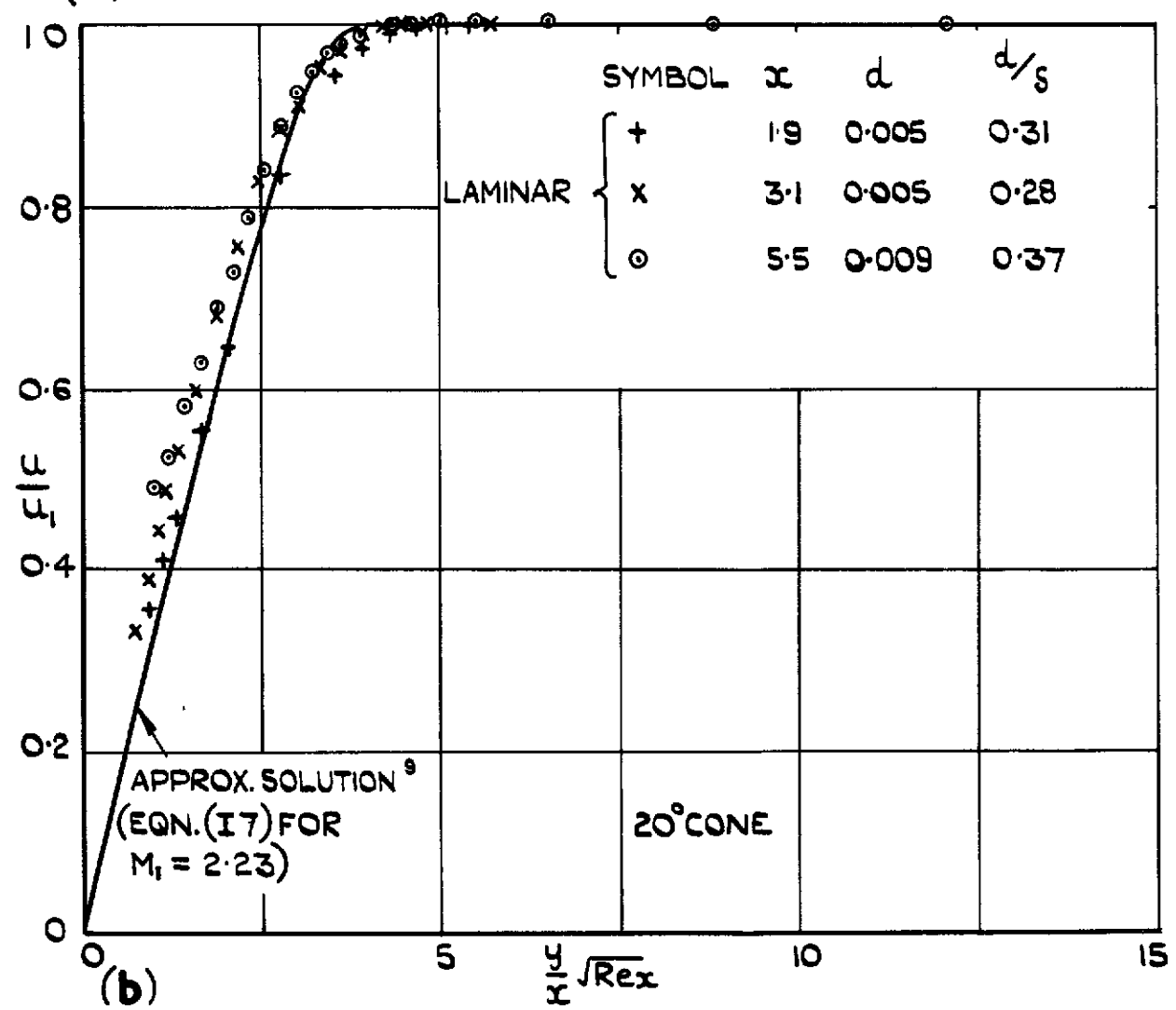

FIG 11(a&b) VELOCITY PROFILES FOR A LAMINAR BOUNDARY LAYER ON 10° AND 20° CONES.

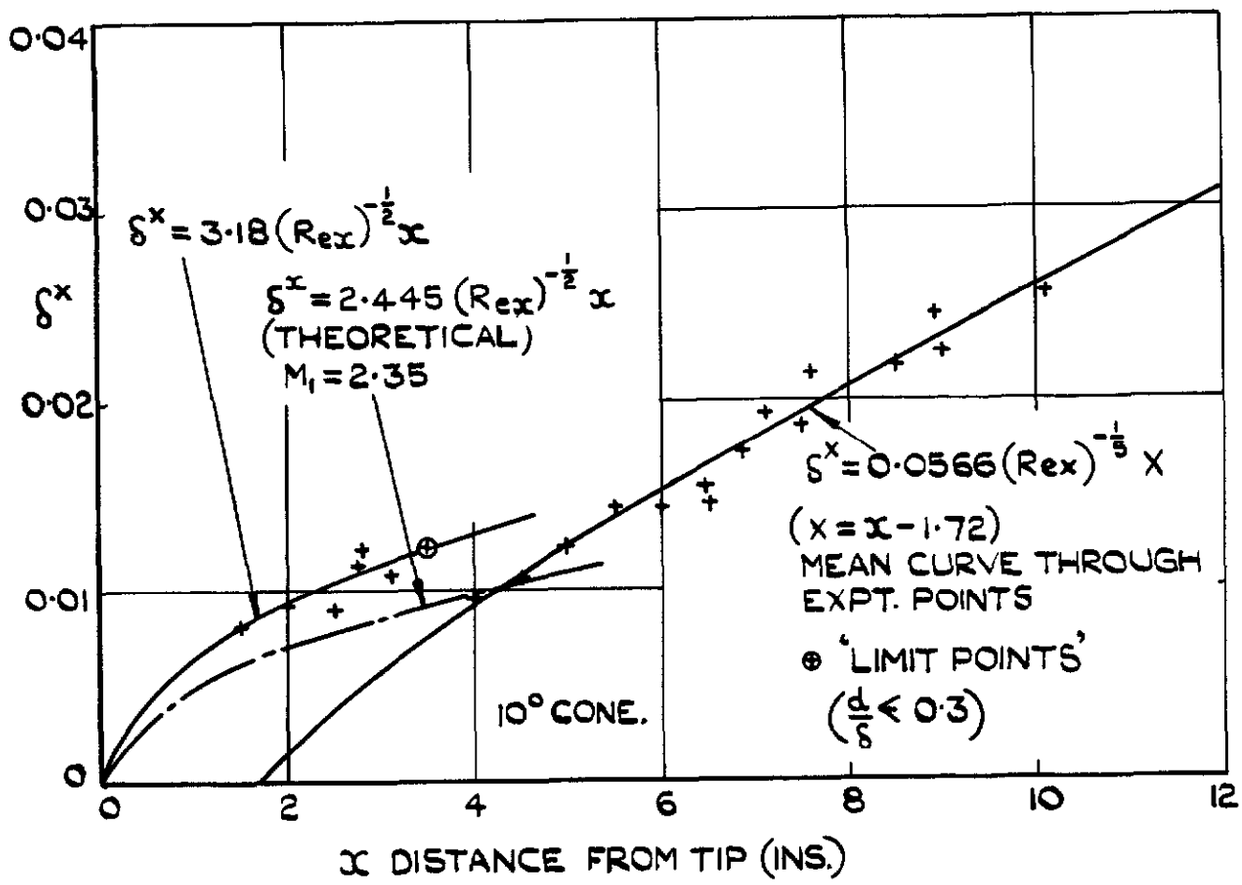

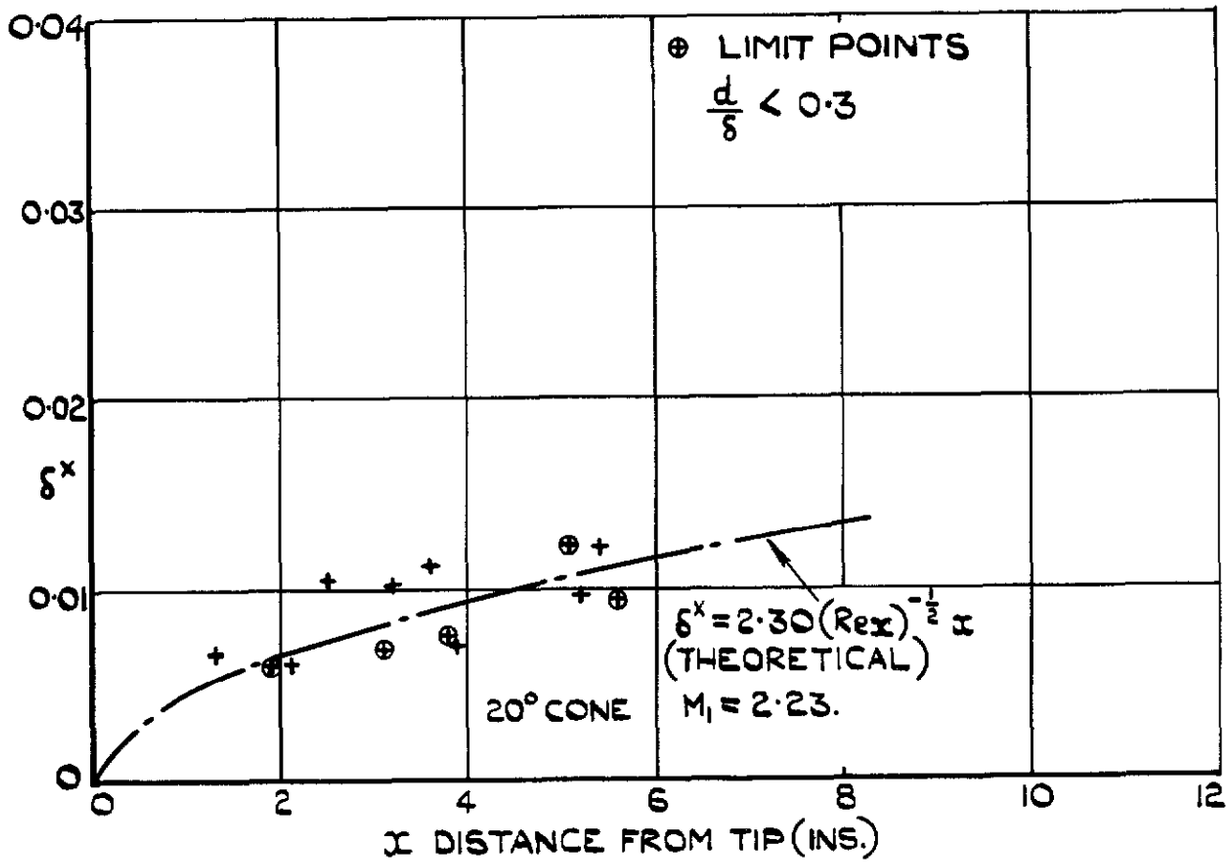

FIG. 12. VARIATION OF DISPLACEMENT THICKNESS ALONG THE CONES.

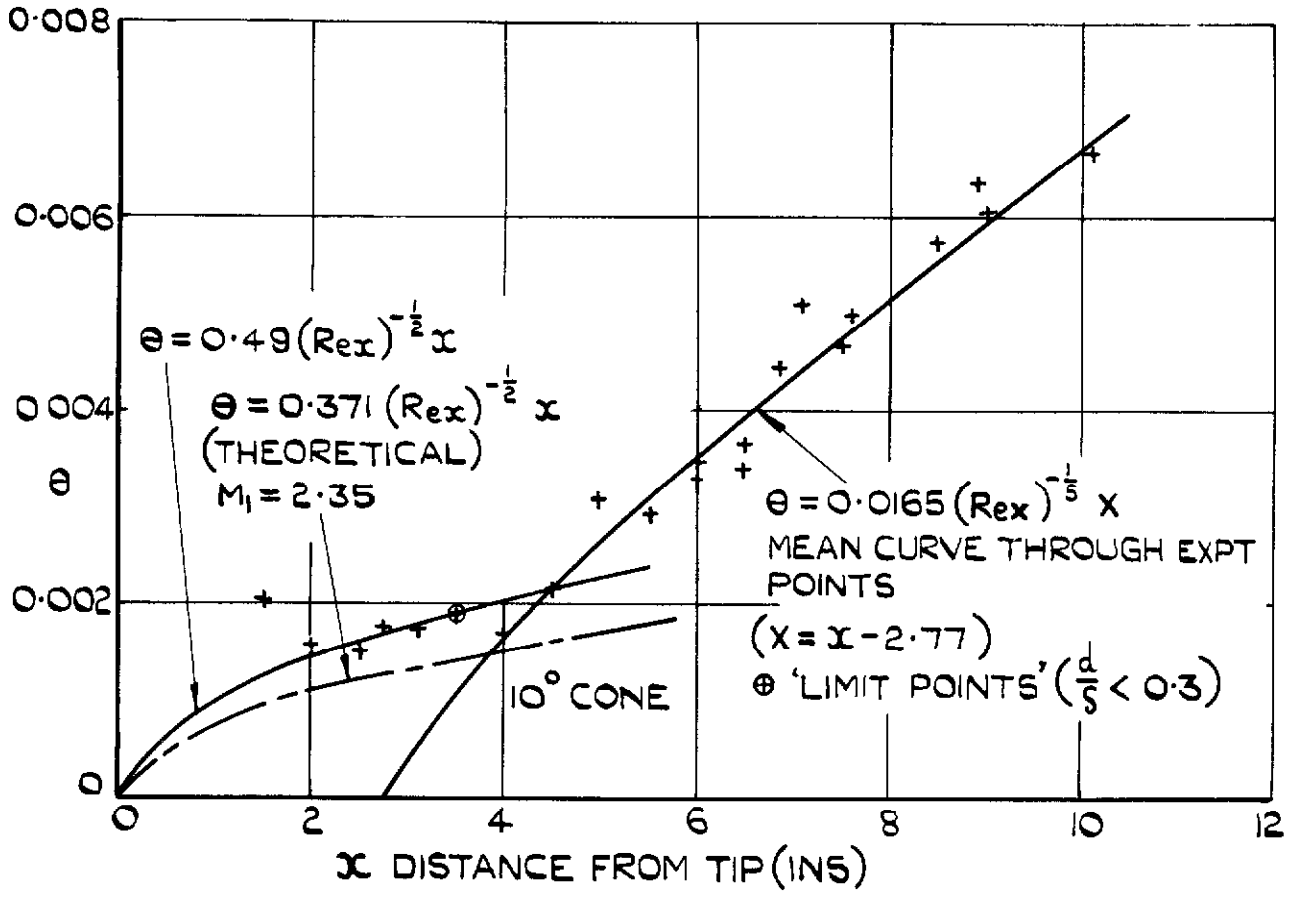

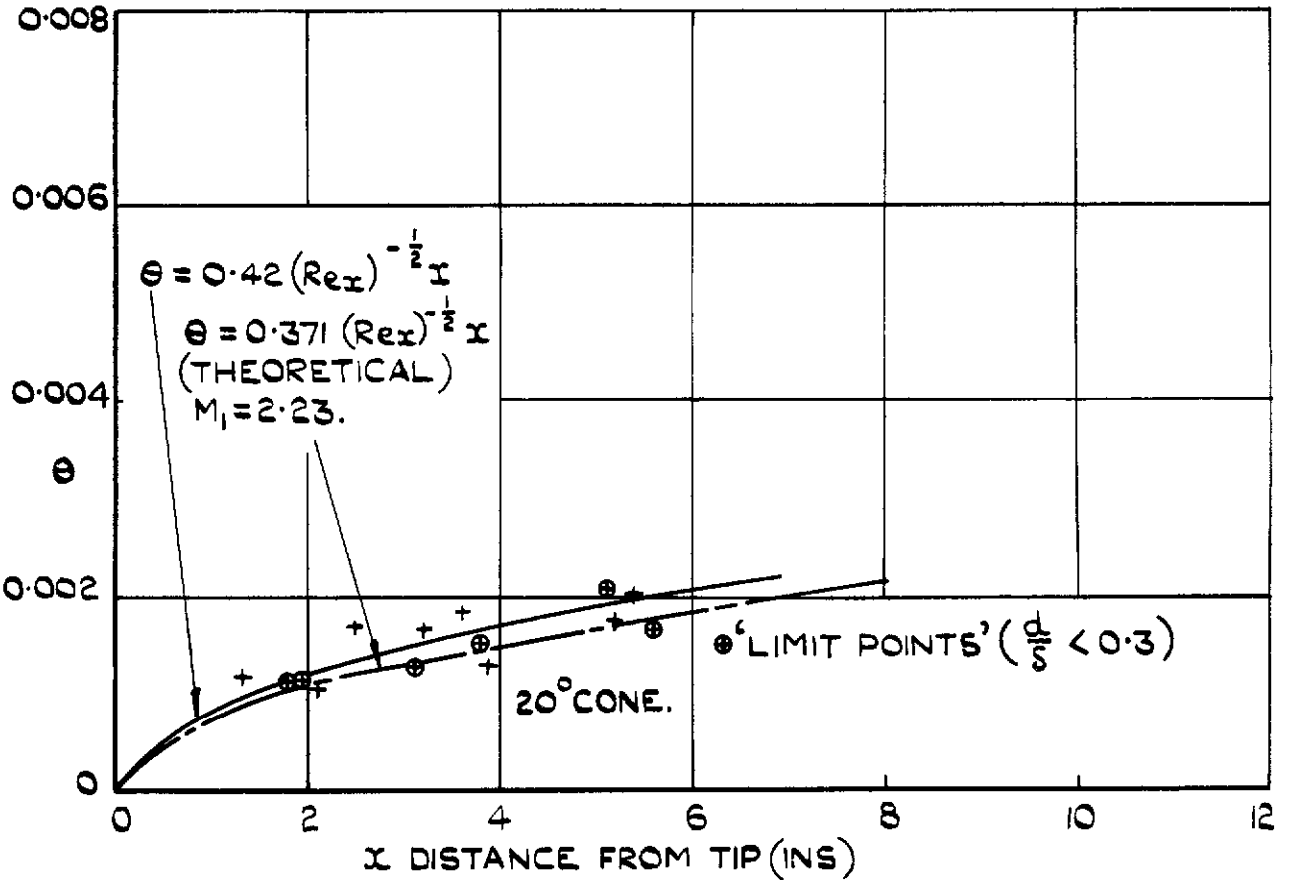

FIG. 13. VARIATION OF MOMENTUM THICKNESS ALONG CONES.

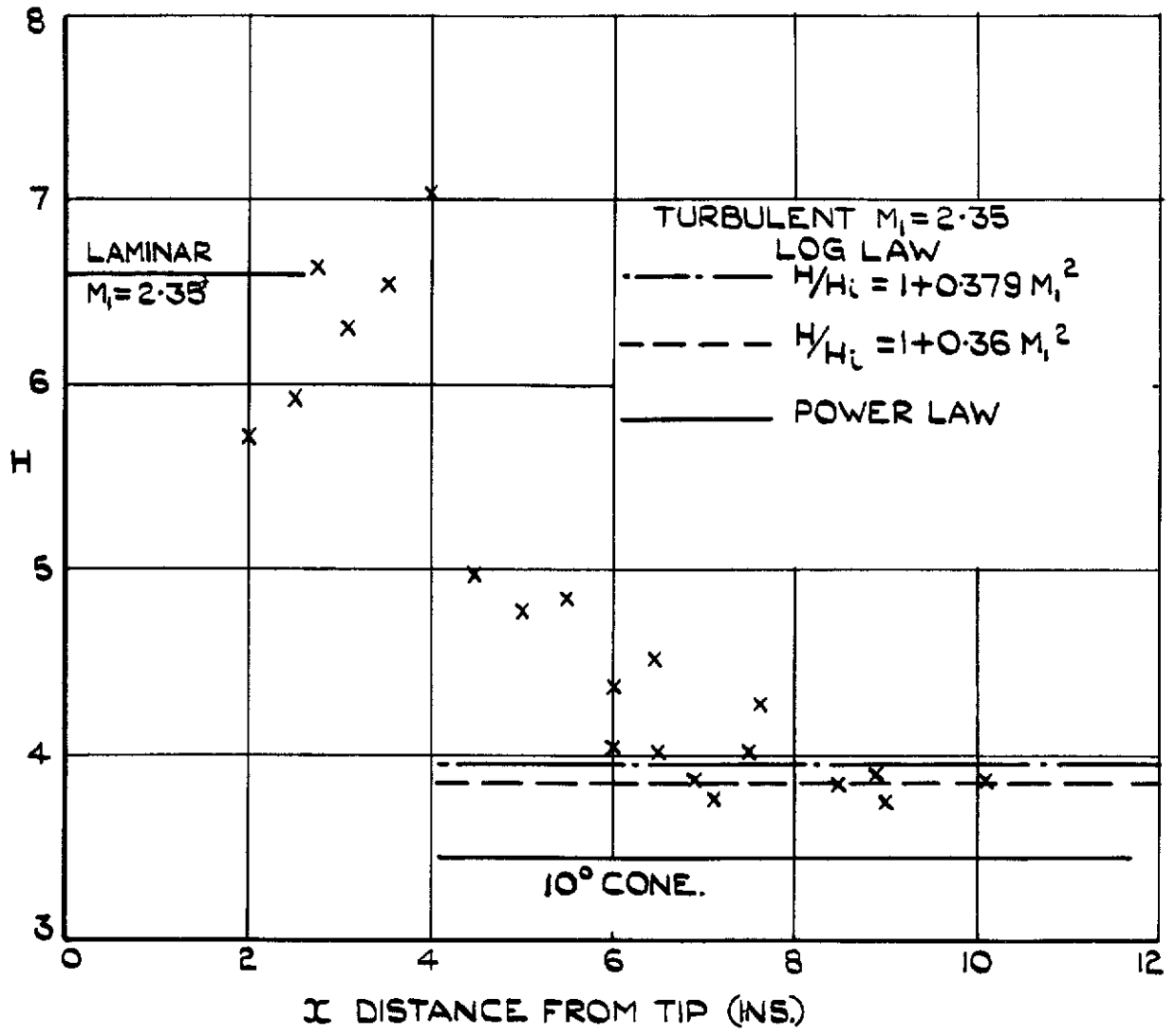

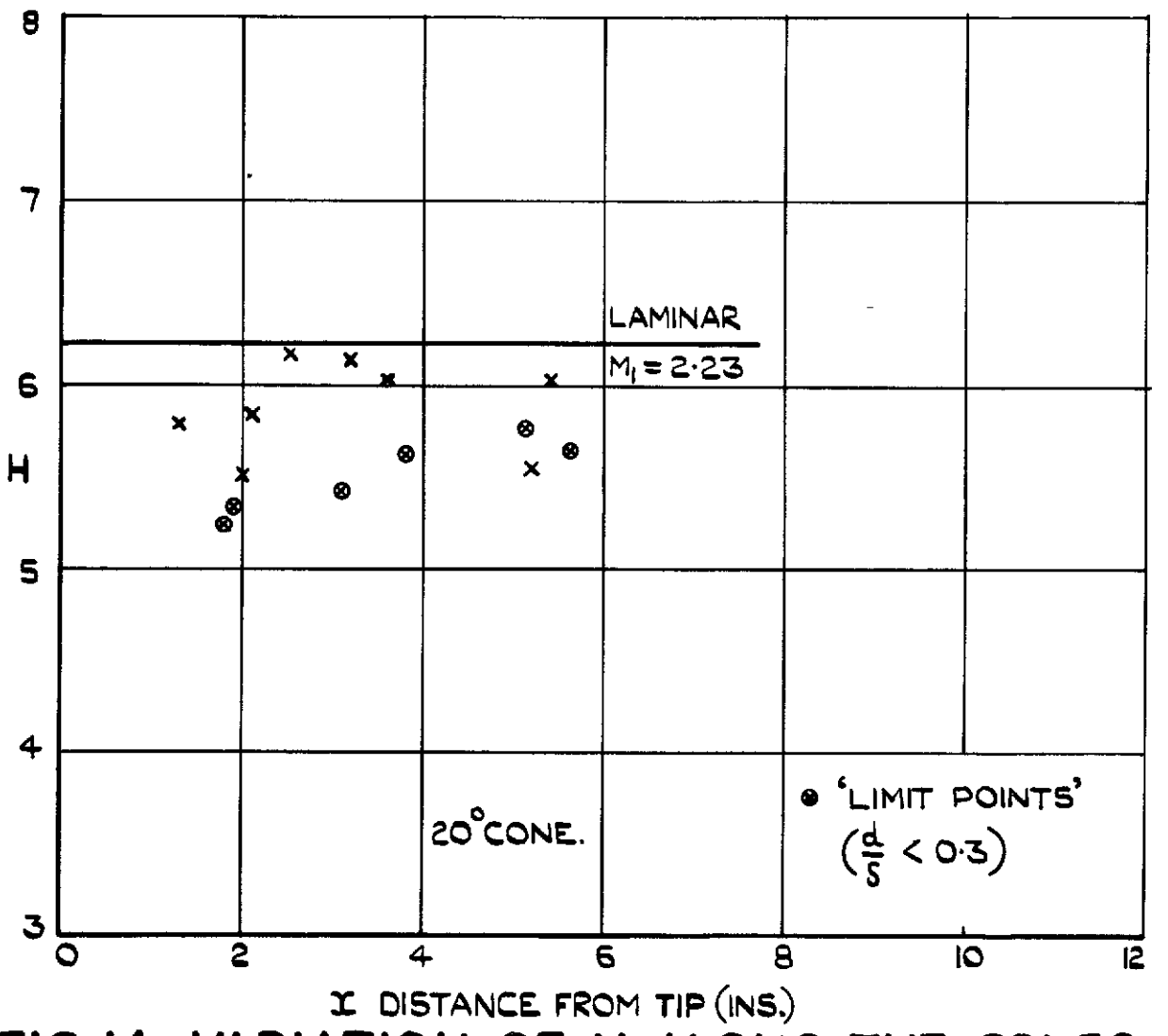

FIG. 14. VARIATION OF H ALONG THE CONES.

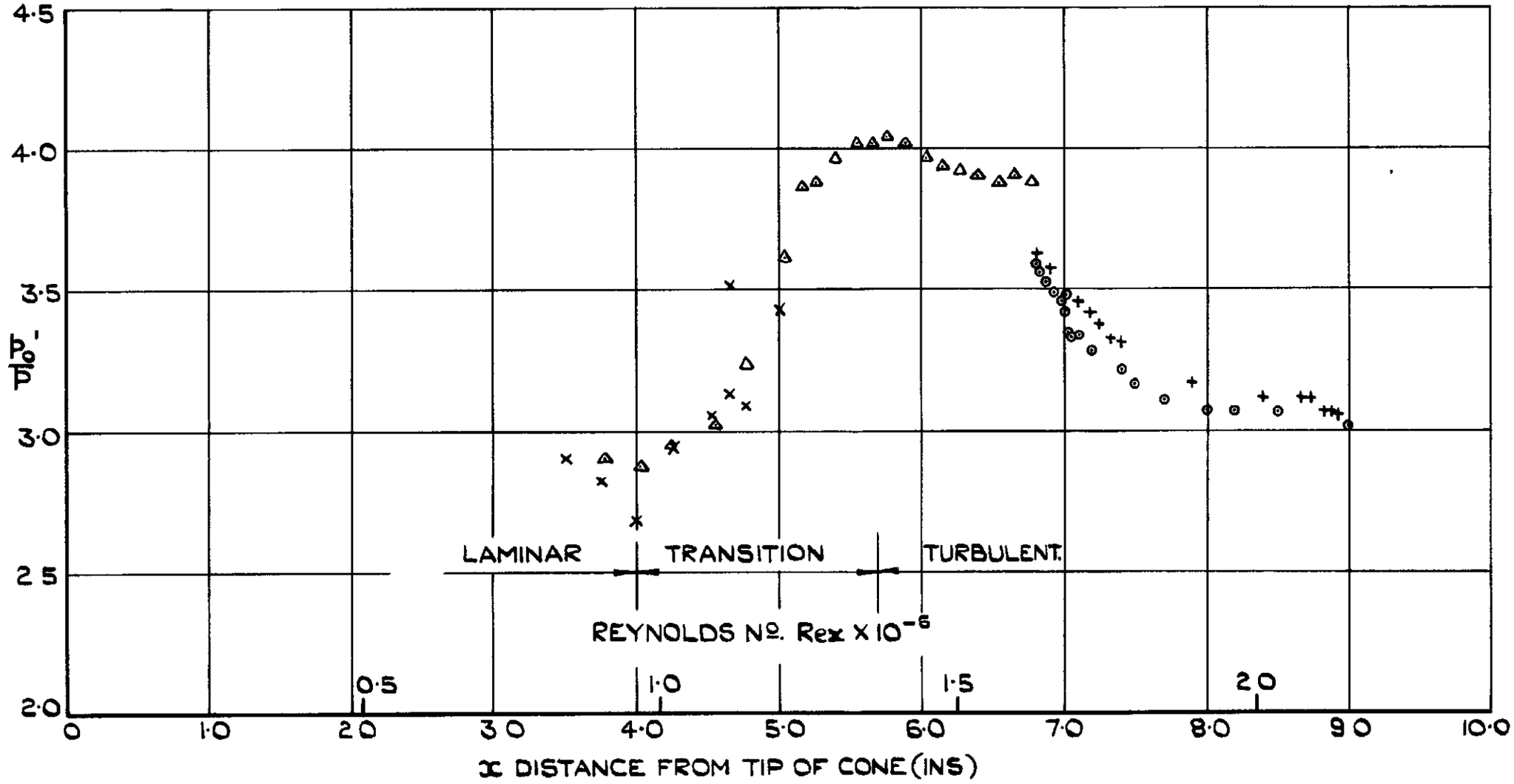

FIG. 15. VARIATION OF PITOT STATIC RATIO ALONG THE 10° CONE (CREEPER PITOT TRAVERSE.)

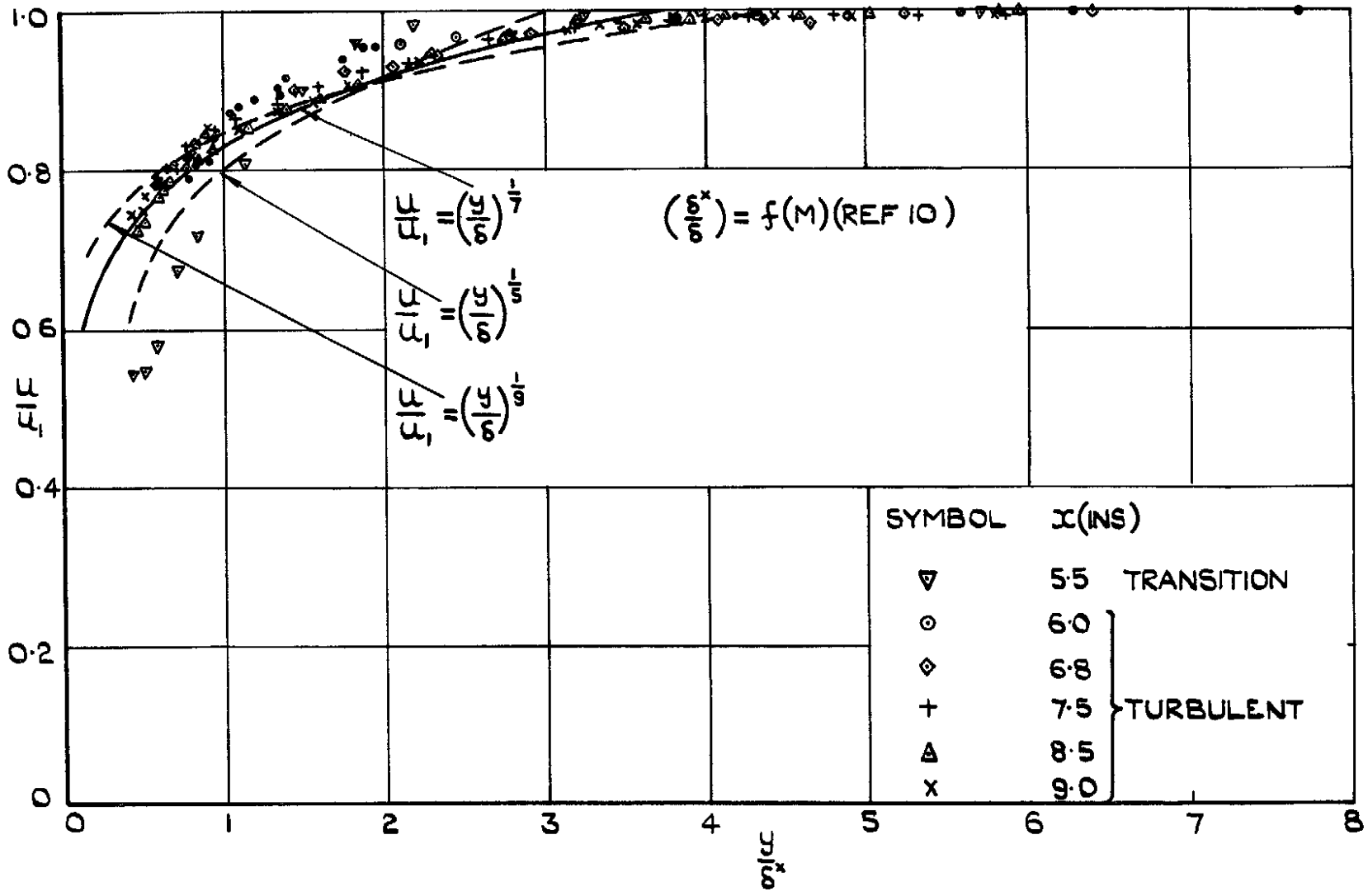

FIG. 16 VELOCITY PROFILES IN BOUNDARY LAYER OVER REAR PORTION OF CONE ($x > 5{\cdot}0''$)

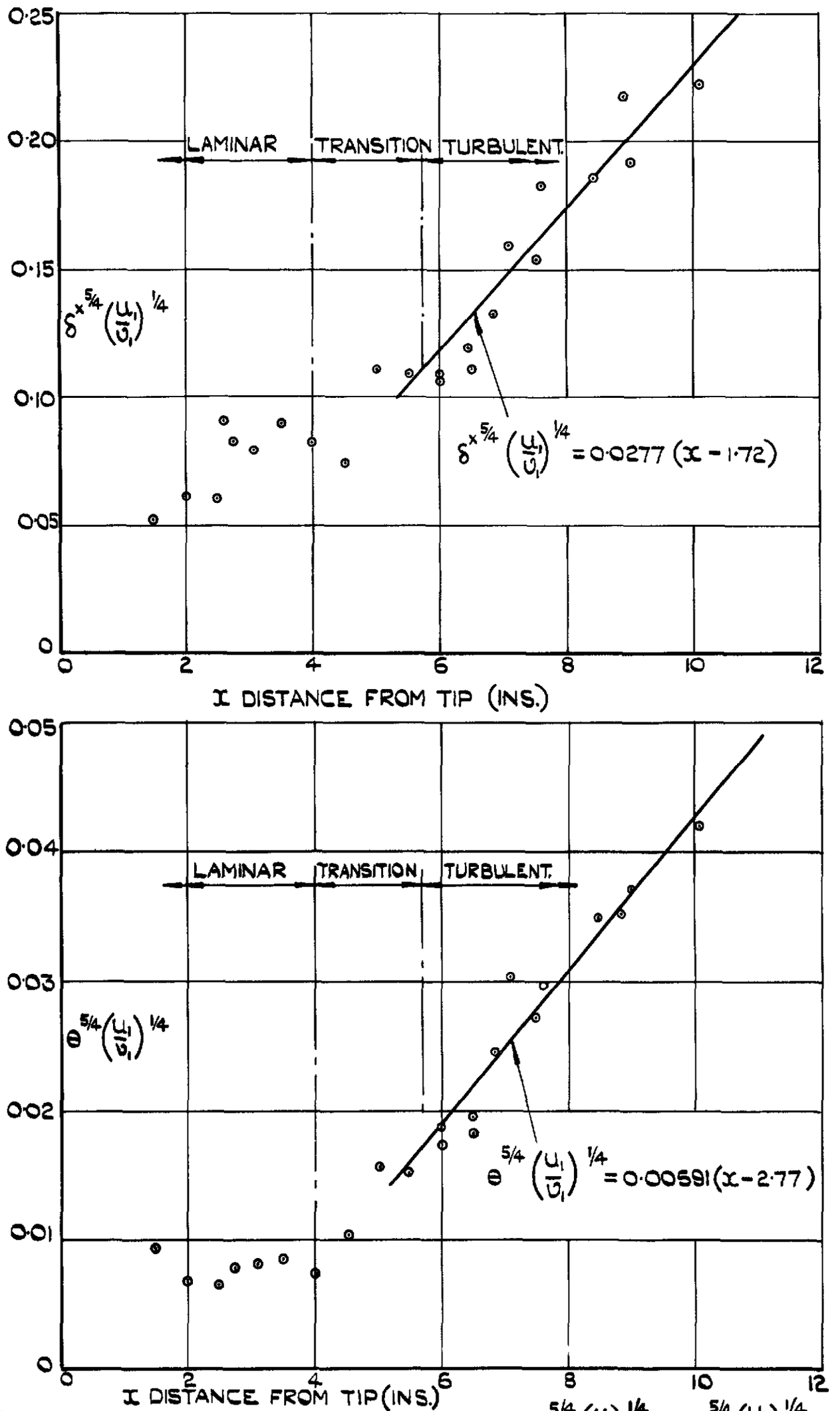

FIG. 17. LINEAR VARIATION OF $\delta^{x^{5/4}}\left(\frac{U_1}{\nu_1}\right)^{1/4}$ & $\theta^{5/4}\left(\frac{U_1}{\nu_1}\right)^{1/4}$ WITH DISTANCE x FROM CONE TIP. (TURBULENT BOUNDARY LAYER 10° CONE).

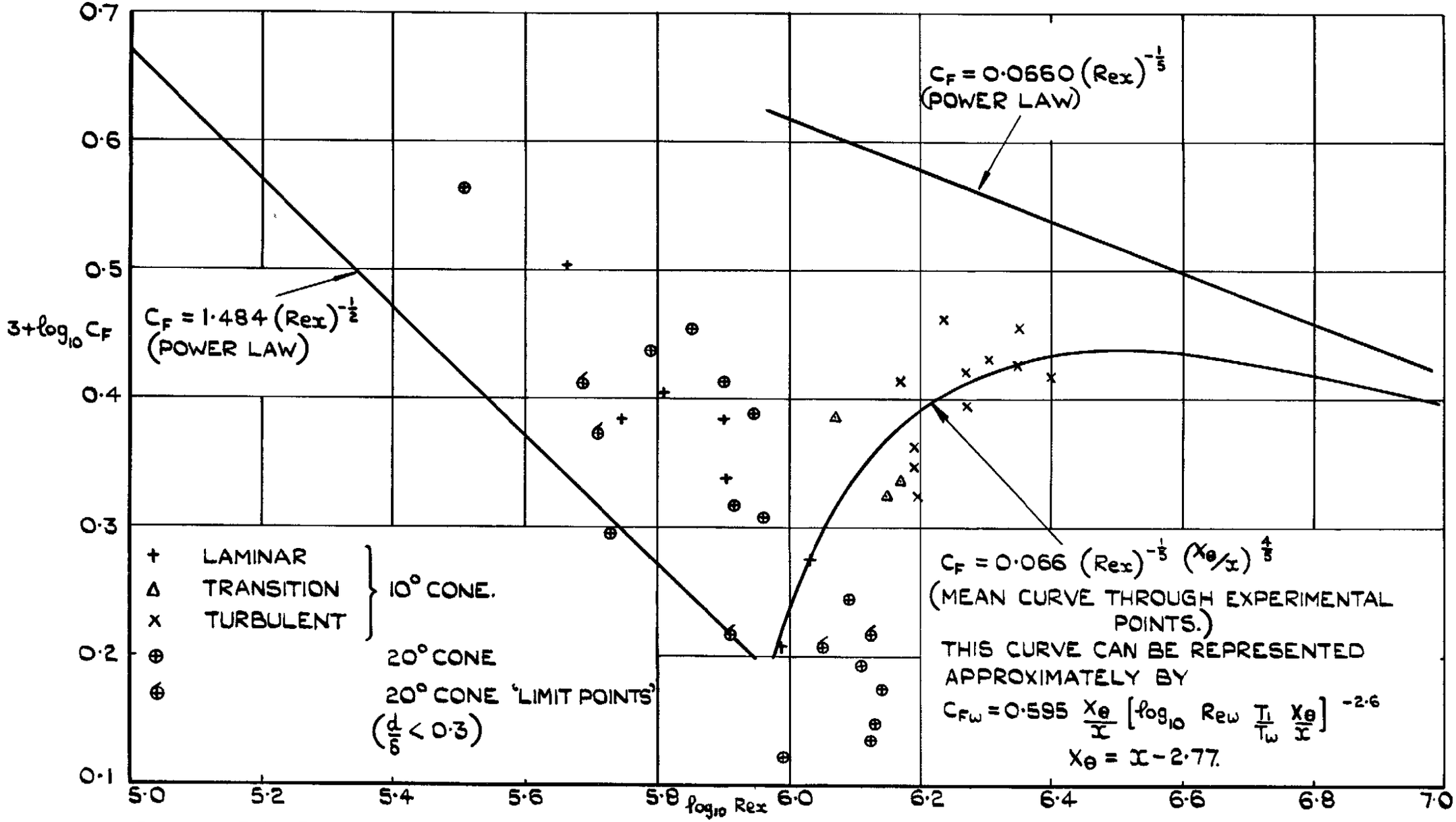

FIG. 18. VARIATION OF OVERALL SKIN FRICTION COEFFICIENT WITH REYNOLDS NUMBER.

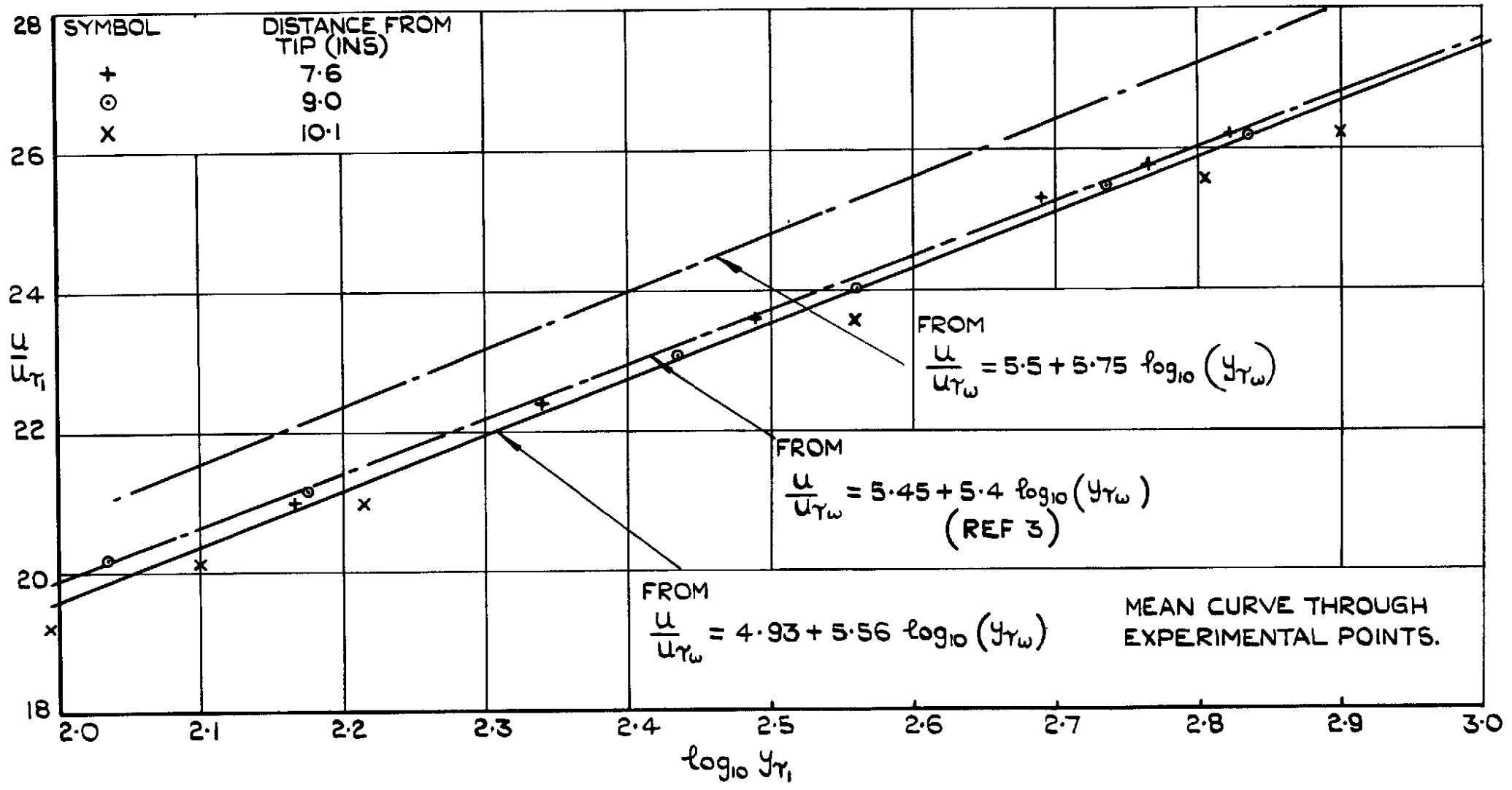

FIG. 19 VELOCITY PROFILES (LOG LAW) FOR THE TURBULENT BOUNDARY LAYER (10° CONE) (SEE SECTION 7·2.)

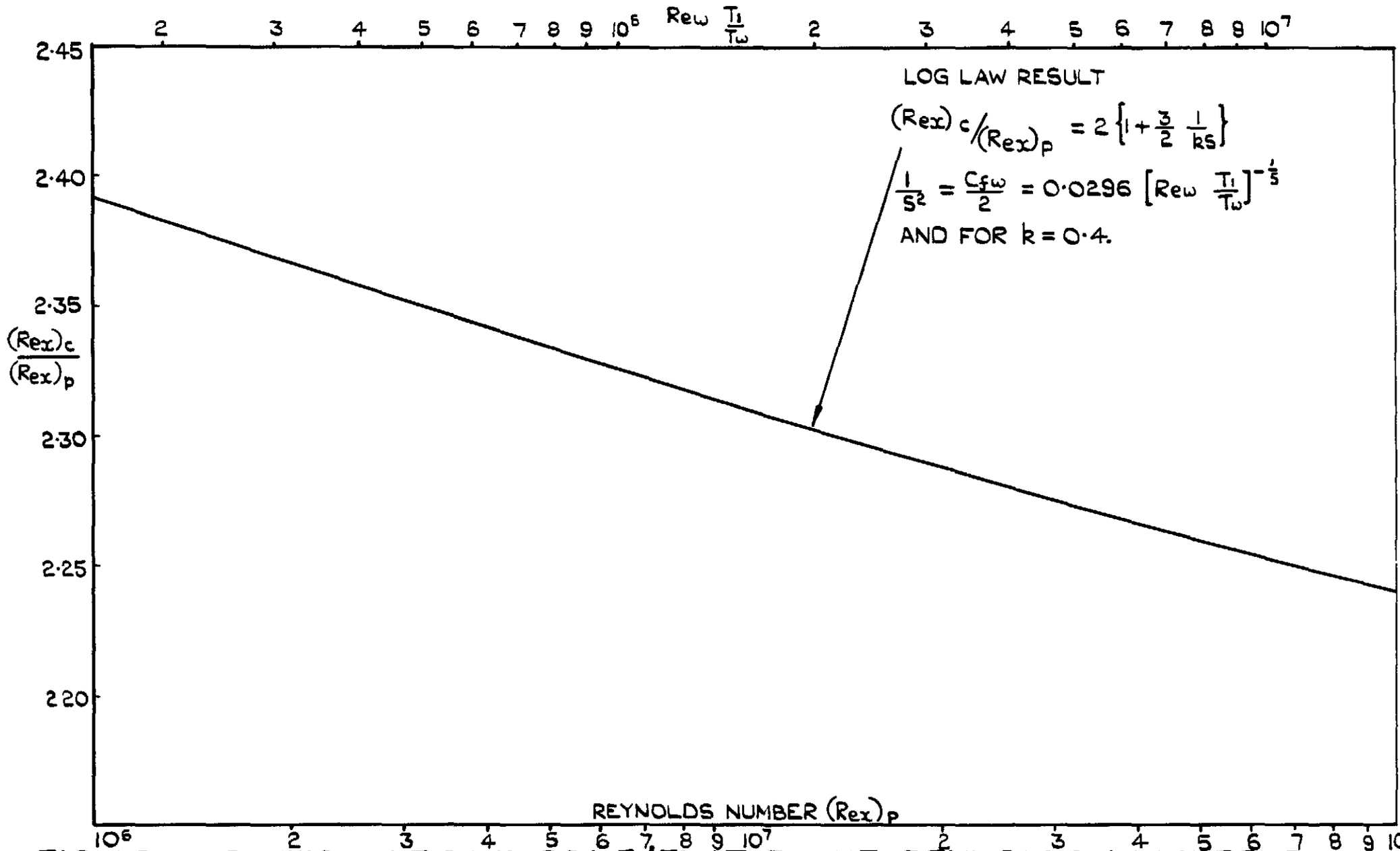

FIG. 20. VARIATION OF THE CONE/FLAT PLATE REYNOLDS NUMBER RATIO $(Rex)_c / (Rex)_p$ FOR IDENTICAL SKIN FRICTION SOLUTIONS.

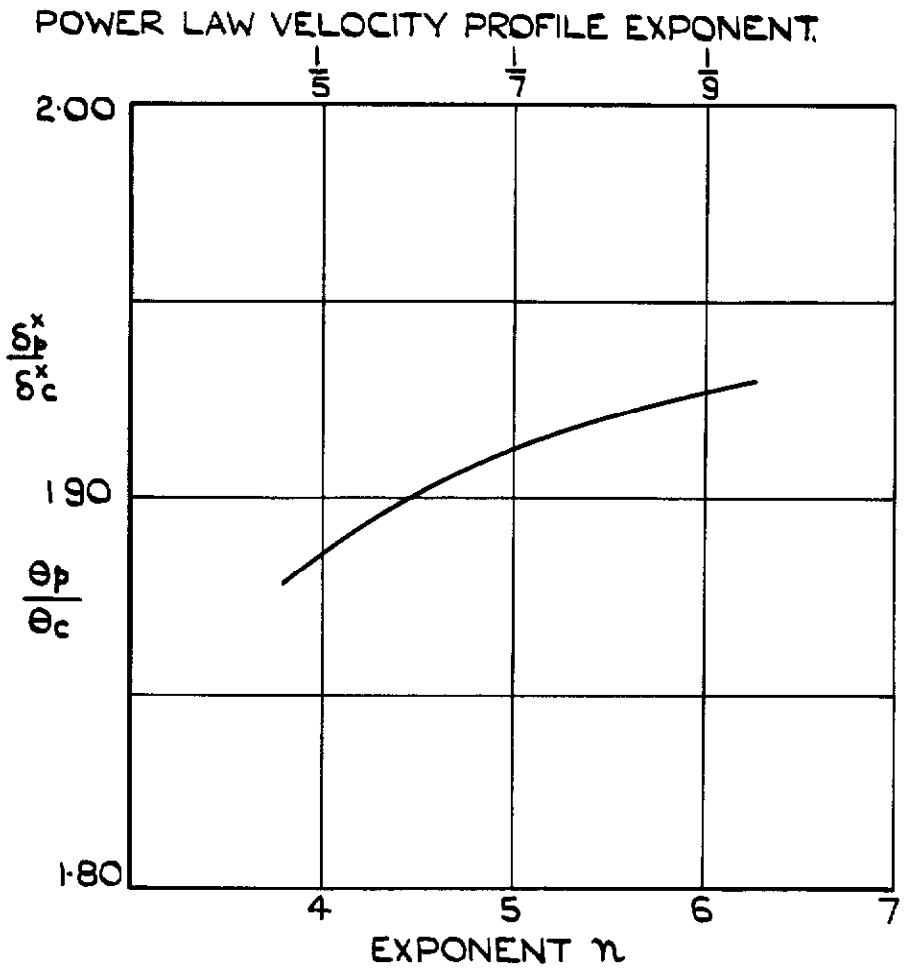

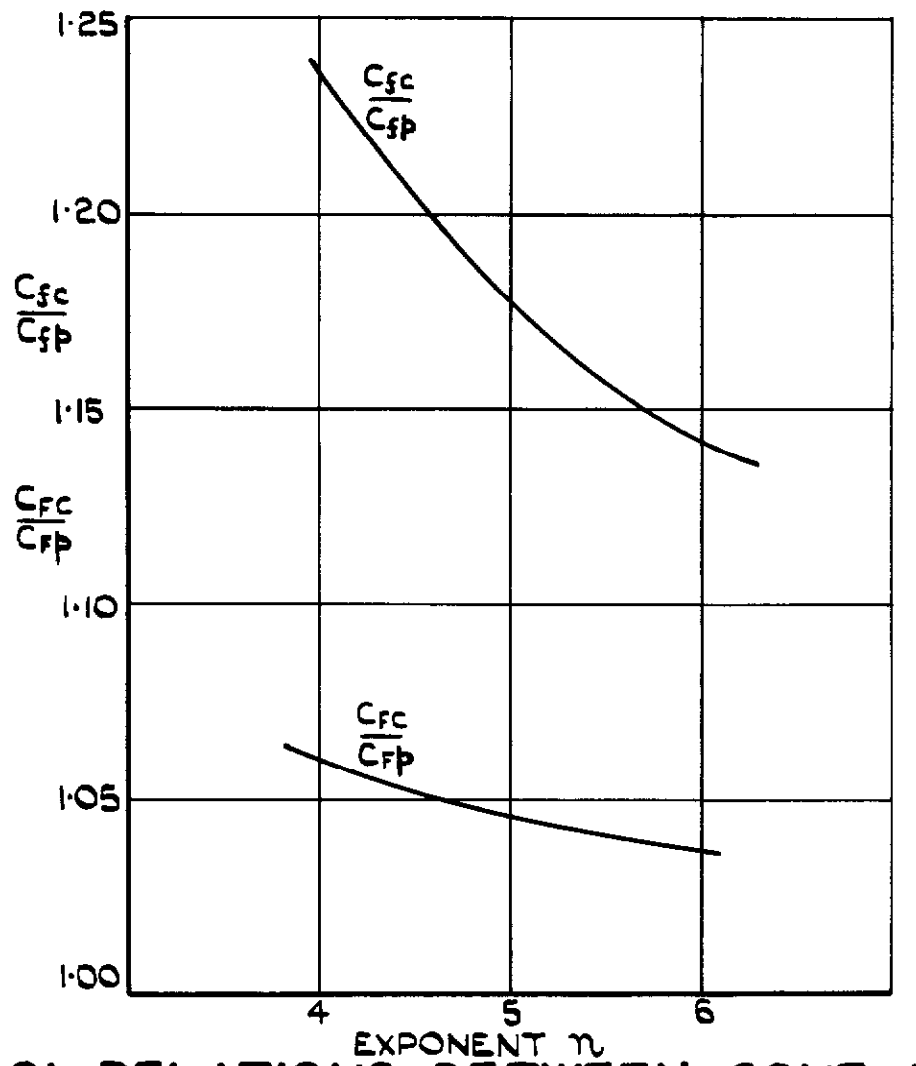

FIG. 21. RELATIONS BETWEEN CONE AND FLAT PLATE TURBULENT BOUNDARY LAYERS USING RESULTS OBTAINED FROM YOUNG'S ANALYSIS.[12]

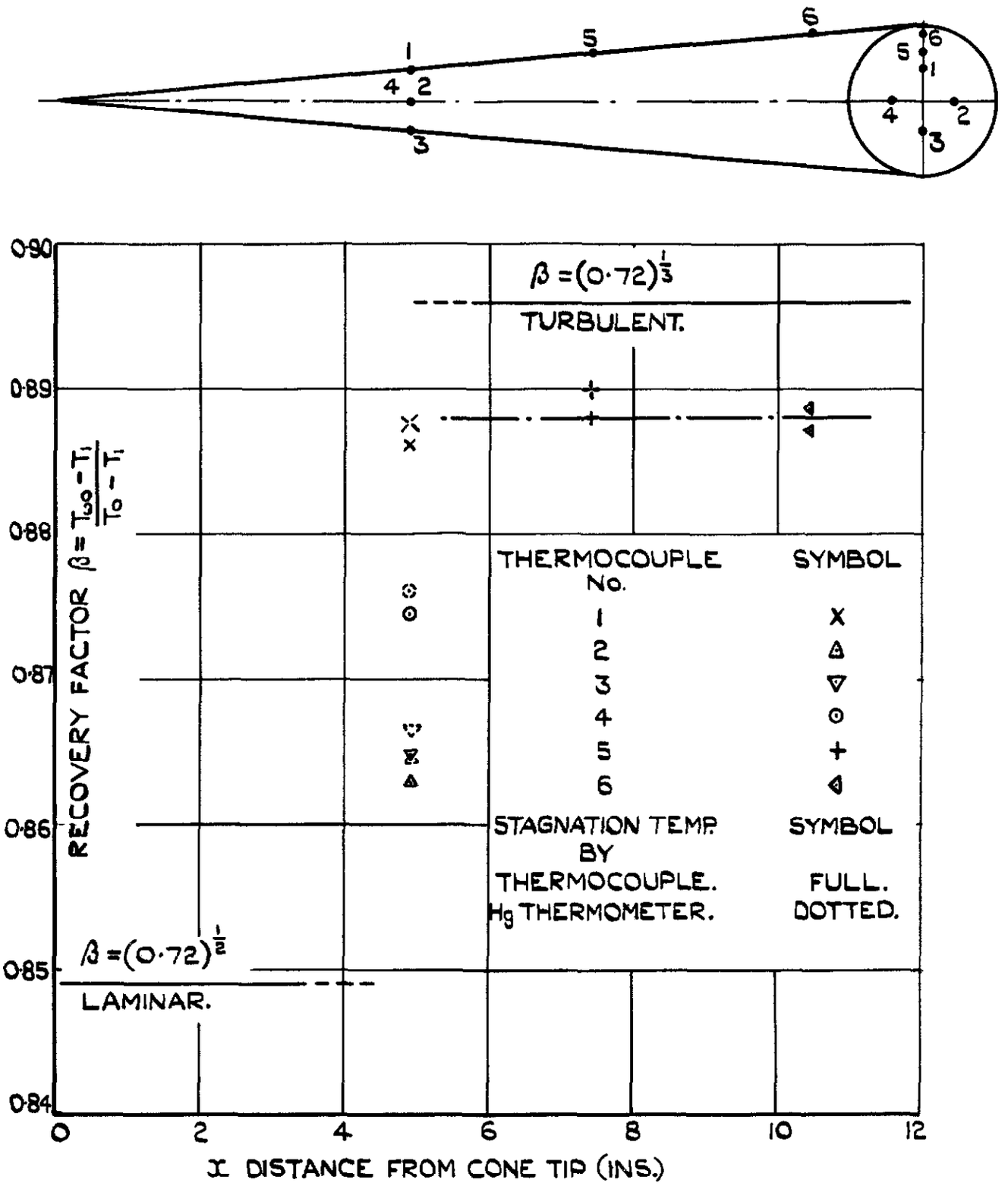

FIG. 22. VARIATION OF RECOVERY FACTOR β ALONG THE 10° PERSPEX CONE.

C.P. No. 264
(17,496)
A.R.C. Technical Report

Published by
HER MAJESTY'S STATIONERY OFFICE

To be purchased from
York House, Kingsway, London W C 2
423 Oxford Street, London W.1
P O Box 569, London S.E 1
13A Castle Street, Edinburgh 2
109 St Mary Street, Cardiff
39 King Street, Manchester 2
Tower Lane, Bristol 1
2 Edmund Street, Birmingham 3
80 Chichester Street, Belfast
or through any bookseller

PRINTED IN GREAT BRITAIN

S.O. Code No. 23-9009-64

C.P. No. 264